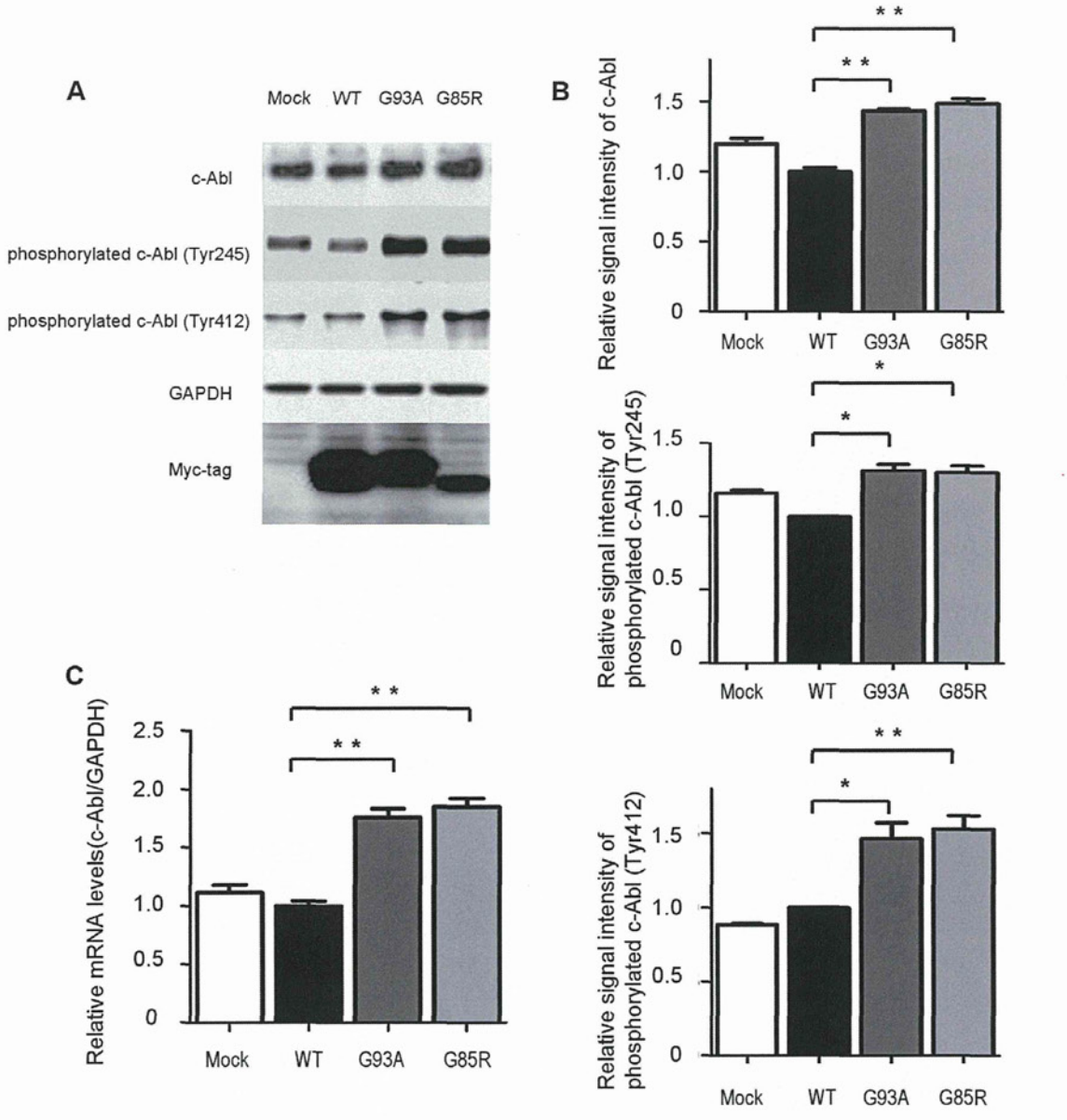

Figure 2. Activation of c-Abl caused by mutant SOD1 overexpression. A: Total c-Abl and phospho-c-Abl (Tyr245 and Tyr412) protein levels in NSC-34 cells overexpressing human wild-type and mutant SOD1 protein were measured by western blotting. GAPDH is shown as a loading control. Cells were cultured with doxycycline (Dox, 2 μg/ml) in serum-free culture medium for 48 h. B: Densitometric analysis (n = 3 per group) of the results shown in Fig. 2A demonstrated that both types of mutant SOD1, G93A and G85R, significantly increased the amount of total c-Abl protein and facilitated phosphorylation at both c-Abl sites, Tyr245 and Tyr412. Data are presented as mean ± SEM. Statistical analysis was performed using 1-way ANOVA with Dunnett's post-hoc test. *$P<0.05$, **$P<0.01$. C: Expression levels of c-Abl mRNA were measured by quantitative RT-PCR in NSC-34 cells overexpressing wild-type or mutant human SOD1 (n = 4 per group). Cells were cultured with doxycycline (Dox, 2 μg/ml) in serum-free culture medium for 48 h. Overexpression of both types of mutant SOD1 significantly increased the c-Abl mRNA level compared with overexpression of wild-type SOD1 ($P<0.01$). Data shown are ratios (mean ± SEM) of the c-Abl mRNA levels in NSC-34 cells overexpressing wild type SOD1 (n = 6). Statistics were evaluated using 1-way ANOVA with Dunnett's post-hoc test. **$P<0.01$.
doi:10.1371/journal.pone.0046185.g002

Dasatinib reduces phosphorylation of c-Abl and the activated form of caspase-3 in G93A mice

To assess the effect of dasatinib on the central nervous system (CNS), we performed western blot analyses using the spinal cords of G93A mice and control littermates treated with dasatinib or vehicle (Fig. 7). The levels of phosphorylated c-Abl (Tyr245) were decreased in a dose-dependent manner in G93A mice treated with dasatinib. In addition, activated caspase-3 was decreased in mice treated with high-dose dasatinib (Fig. 7). Quantification of immunofluorescence revealed that phosphorylated c-Abl (Tyr412) levels were significantly decreased in dasatinib-treated G93A mice at doses of 15 mg/(kg·day) or higher compared with vehicle-treated control mice ($P<0.01$) (Fig. S2). These results suggest that dasatinib protects motor neurons from mutant SOD1-induced neuronal cell death by inhibiting apoptosis.

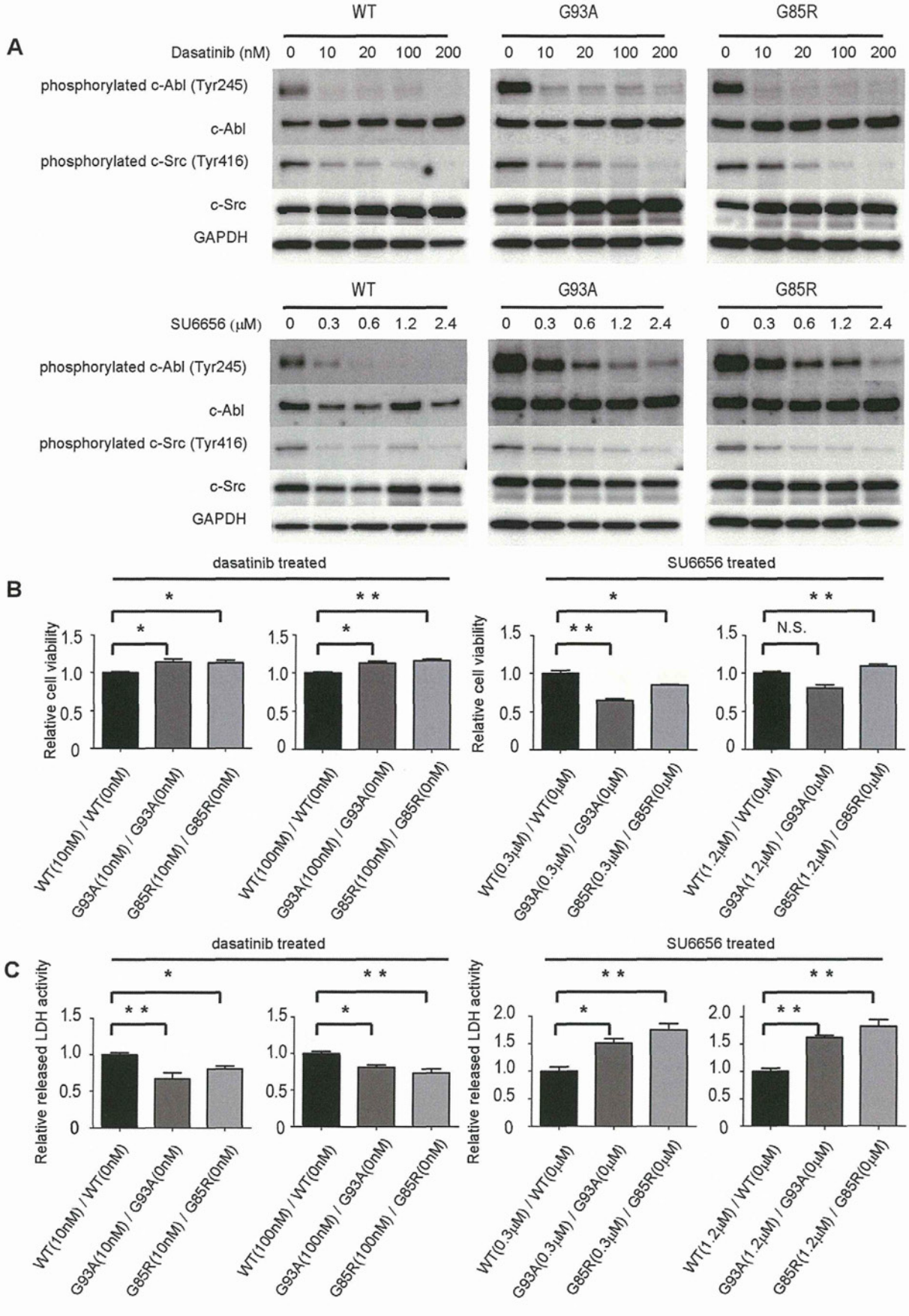
A
WT
G93A
G85R
Dasatinib (nM) 0 10 20 100 200
phosphorylated c-Abl (Tyr245)
c-Abl
phosphorylated c-Src (Tyr416)
c-Src
GAPDH
SU6656 (μM) 0 0.3 0.6 1.2 2.4
B
dasatinib treated
SU6656 treated
Relative cell viability
N.S.
WT(10nM) / WT(0nM)
G93A(10nM) / G93A(0nM)
G85R(10nM) / G85R(0nM)
WT(100nM) / WT(0nM)
G93A(100nM) / G93A(0nM)
G85R(100nM) / G85R(0nM)
WT(0.3μM) / WT(0μM)
G93A(0.3μM) / G93A(0μM)
G85R(0.3μM) / G85R(0μM)
WT(1.2μM) / WT(0μM)
G93A(1.2μM) / G93A(0μM)
G85R(1.2μM) / G85R(0μM)
C
Relative released LDH activity

Figure 3. Dasatinib reduces cytotoxicity of mutant SOD1s in NSC-34 cells. A: Protein levels of phosphorylated c-Abl (Tyr245), c-Abl, phosphorylated c-Src (Tyr416), c-Src, and GAPDH in NSC-34 cells overexpressing human wild-type or mutant SOD1s treated with various concentrations of dasatinib or SU6656 were measured by western blot. Cells were cultured in serum-free culture medium with doxycycline (Dox, 2 μg/ml), and western blot was performed at 24 h after dasatinib or SU6656 addition. B: Cells were grown in 96-well collagen-coated plates (3,500 cells per well) with doxycycline (Dox, 2 μg/ml) in culture medium containing 10% FBS for 16 h. Culture medium was then replaced with 1% FBS-containing medium including the indicated concentrations of dasatinib and 2 μg/ml doxycycline (Dox). MTS assays were performed at 24 h after addition of dasatinib or SU6656. Viability was measured as the level of absorbance at 490 nm. Absorbance at 490 nm was expressed as the mean ± SEM (n = 6). Ratios of relative cell viability based on the MTS assay were calculated to determine the beneficial effect of dasatinib in mutant cells overexpressing SOD1s. Absorbance at 490 nm was standardized relative to the absorbance at each corresponding time point for 0 nM dasatinib. Cell viability assay confirmed that dasatinib significantly reduced the cytotoxicity of mutant SOD1s, whereas SU6656 did not. Statistics were evaluated using 1-way ANOVA with Dunnett's post-hoc test. *$P<0.05$, **$P<0.01$. C: Cells were grown in 96-well collagen-coated plates (3,500 cells per well) with doxycycline (Dox, 2 μg/ml) in culture medium containing 10% FBS for 16 h. Culture medium was then replaced with 1% FBS-containing medium with the indicated concentrations of dasatinib and 2 μg/ml doxycycline (Dox). LDH assays were performed at 24 h after dasatinib or SU6656 addition. Cytotoxicity was measured as the level of absorbance at 490 nm. Ratios of relative LDH release were calculated to determine the beneficial effect of dasatinib in mutant cells overexpressing SOD1s. Absorbance at 490 nm was standardized relative to the absorbance at each corresponding time point for 0 nM dasatinib. LDH assay confirmed that dasatinib significantly reduced the cytotoxicity of mutant SOD1s, whereas SU6656 did not. Values represent the mean ± SEM of the ratio of LDH release (n = 4). Statistics were evaluated using 1-way ANOVA with Dunnett's post-hoc test. *$P<0.05$, **$P<0.01$.
doi:10.1371/journal.pone.0046185.g003

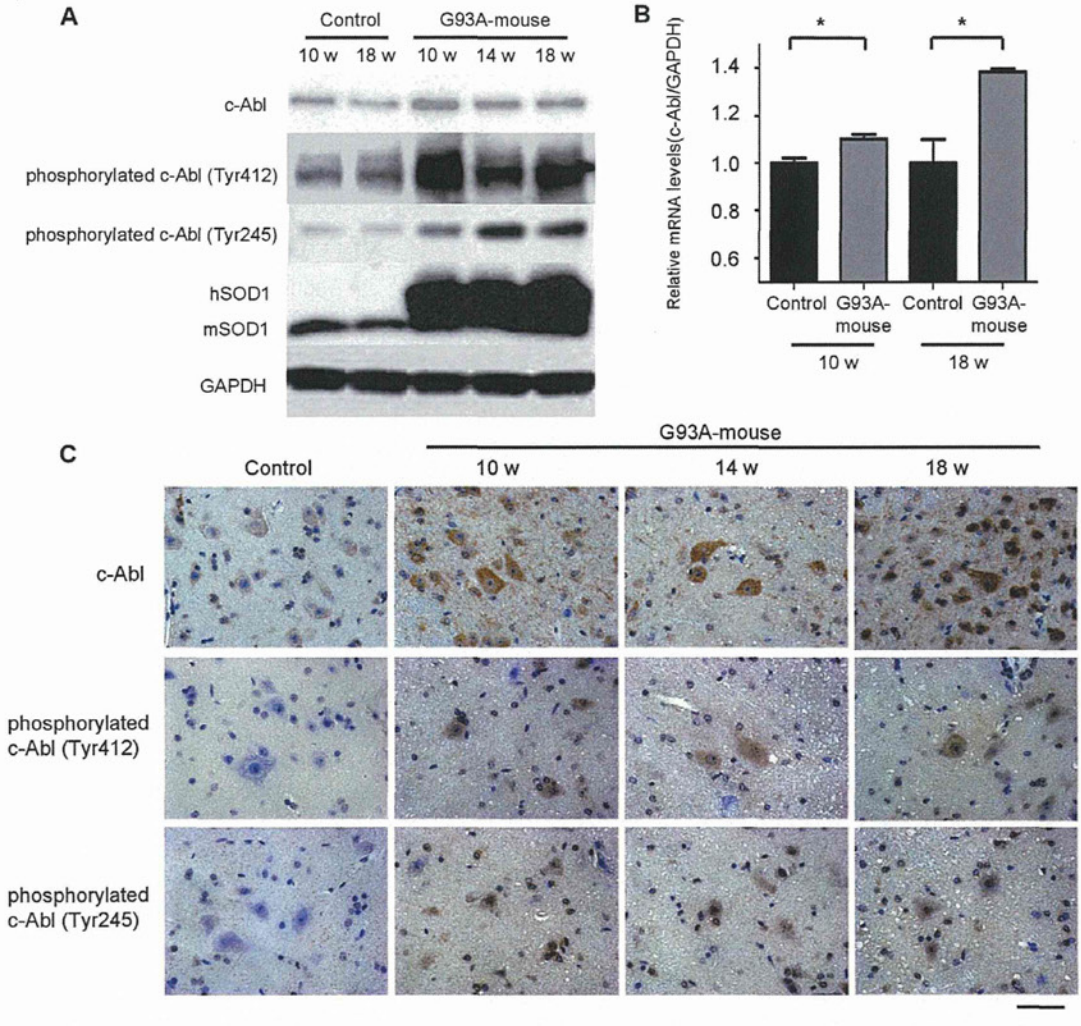

Figure 4. c-Abl upregulation and activation in G93A mice. A: Protein levels of phosphorylated c-Abl (Tyr245 and Tyr412) and c-Abl were analyzed by western blot using spinal cord protein extracts from control non-transgenic and G93A mice at the indicated ages. GAPDH is shown as a loading control. hSOD1 and mSOD1 indicate human SOD1 and mouse endogenous SOD1, respectively. B: c-Abl mRNA levels in the spinal cords of G93A mice and control littermates (age 10 and 18 weeks; n = 4 per group) were measured by quantitative RT-PCR. Data shown are the ratios of the c-Abl mRNA level in each group relative to that in control littermates. c-Abl mRNA was significantly increased in the spinal cords of G93A mice in both age groups compared with control littermates ($P<0.05$). Data are presented as mean ± SEM. Statistics were evaluated using Student's *t* test. *$P<0.05$. C: Distribution of total and phosphorylated c-Abl proteins was analyzed by immunohistochemical staining of paraffin-embedded spinal cord sections from G93A mice (10, 14, and 18 weeks old) and control littermates (20 weeks old) using antibodies directed against c-Abl, phosphorylated c-Abl (Tyr245), and phosphorylated c-Abl (Tyr412). Scale bar: 50 μm.
doi:10.1371/journal.pone.0046185.g004

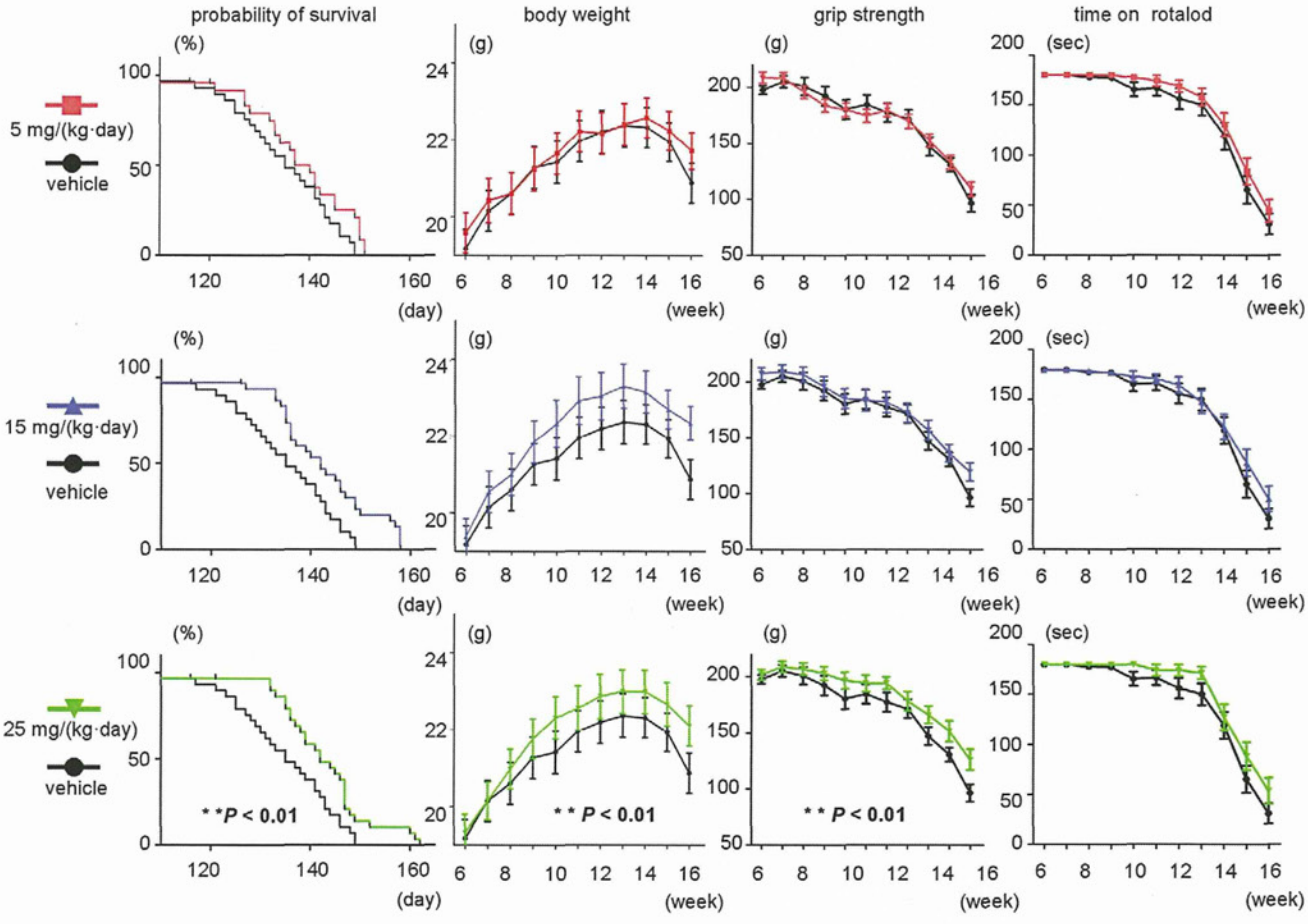

Figure 5. The effect of dasatinib on survival and disease progression in G93A mice. Rotarod activity, grip strength, body weight, and survival rate in G93A mice with or without dasatinib treatment (0, 5, 15, and 25 mg/(kg·day)). Survival of G93A mice was improved by dasatinib at a dose of 25 mg/(kg·day) compared with vehicle treatment (Log-rank test, $P<0.01$, 25 mg/(kg·day) vs. vehicle), whereas a lower dose of dasatinib (5 mg/(kg·day)) had no significant effect on life span. Weight loss was also ameliorated by dasatinib at a dose of 25 mg/(kg·day) compared with vehicle treatment (2-way ANOVA, $P<0.01$, 25 mg/(kg·day) vs. vehicle). The administration of dasatinib at 25 mg/(kg·day) similarly ameliorated grip strength (2-way ANOVA, $P<0.01$, 25 mg/(kg·day) vs. vehicle). The difference in physical function between the groups as assessed by rotarod was not significant by 2-way ANOVA, although a beneficial tendency of dasatinib was observed.
doi:10.1371/journal.pone.0046185.g005

Upregulation and activation of c-Abl in sporadic ALS

To investigate the implications of c-Abl in human sALS, we next examined the expression and activation levels of c-Abl in post-mortem spinal cord specimens from sALS cases. Lumbar spinal cord tissue from 3 sALS cases and 3 control cases with no neurodegenerative disease were used for immunohistochemical and western blot analyses. Western blotting revealed a more than 3-fold increase in c-Abl protein in sALS (Fig. 8A, B). More intense c-Abl immunohistochemical signal was also observed in lumbar spinal cord sections from sALS cases compared to control cases (Fig. 8C). Immunoreactivity of phosphorylated c-Abl (Tyr245 and Tyr412) in motor neurons was also increased in sALS specimens compared to controls (Fig. 8C). These findings indicate that upregulation and activation of c-Abl in motor neurons occurs not only in G93A mice but also in sALS patients.

Discussion

In this study, we established mouse motor neuronal cell lines in which either wild-type or mutant SOD1s were induced by doxycycline. We found that overexpression of mutant SOD1s induced expression and activation of c-Abl and decreased cell viability in a mouse motor neuron cell model. Furthermore, dasatinib, a BBB-permeable inhibitor of c-Abl, attenuated c-Abl phosphorylation and reduced the cytotoxicity induced by overexpression of mutant SOD1s. Dasatinib is a dual kinase inhibitor against c-Abl and c-Src family tyrosine kinases [31]. To clarify the specificity of c-Abl for the motor neuronal cytotoxicity, we performed cell proliferation and cell death assays with or without SU6656, which preferentially inhibits c-Src compared to c-Abl [32]. As shown in Fig. 3, dasatinib ameliorated the cytotoxic effects of mutant SOD1, whereas SU6656 did not. This finding indicates that c-Abl inhibition delays motor neuronal cell death caused by mutant SOD1. Our results are consistent with previous studies demonstrating that some apoptotic stimuli, such as amyloid beta and oxidative stress, also caused c-Abl activation [25,29], and that imatinib, another c-Abl inhibitor, had an inhibitory effect on apoptotic pathways [28].

Our study also provides evidence that c-Abl upregulation and activation occur in the lumbar spinal cord of G93A mice. c-Abl activation has recently been reported to occur in animal models of Niemann-Pick type C and Alzheimer's disease [28,33], but the present report is the first to demonstrate c-Abl activation in an animal model of ALS. Throughout the disease course of G93A

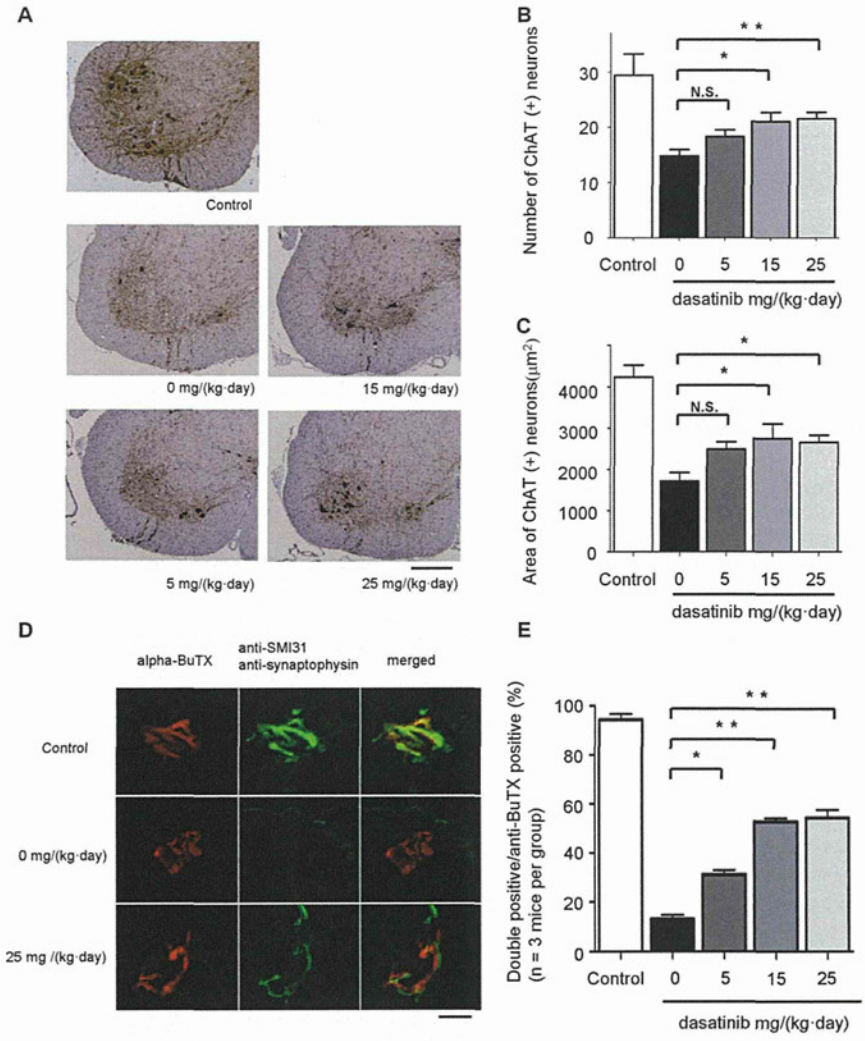

Figure 6. The effect of dasatinib on motor neuron survival in G93A mice. A: Spinal cord (L1-3) specimens from 120-day-old mice were immunostained with anti-ChAT antibody. The mice were administered the indicated amounts of dasatinib daily from postnatal day 56 to day 120 (n = 8 mice per group). Scale bar: 250 μm. B: The number of ChAT-positive neurons in the sections described in Fig. 6A was counted using Image J software. Dasatinib prevented the loss of ChAT-positive motor neurons in the ventral horn of G93A mice at doses of 15 mg/(kg·day) ($P<0.05$) and 25 mg/(kg·day) ($P<0.01$). Statistics were evaluated using 1-way ANOVA with Dunnett's post-hoc test. *$P<0.05$, **$P<0.01$. C: The area of ChAT-positive neurons in the sections described in Fig. 6A was determined using Image J software. Dasatinib increased the size of motor neuron cell bodies at doses of 15 and 25 mg/(kg·day) ($P<0.05$). Statistics were evaluated using 1-way ANOVA with Dunnett's post-hoc test. *$P<0.05$. D: To investigate the innervation status of NMJs, frozen quadriceps femoris specimens from 120-day-old mice were stained with alpha-BuTX (red) and anti-synaptophysin (green) or anti-SMI31 (green) antibodies. Representative NMJs visualized with the confocal laser scanning microscopy are shown. The mice were administered the indicated amounts of dasatinib daily from postnatal day 56 to day 120. Scale bar: 10 μm. E: The ratio of double-immunostained innervated NMJs to total NMJs is summarized. One hundred immunostained NMJs were investigated in each dasatinib-treated mouse (n = 3 mice per group). Dasatinib significantly ameliorated the destruction of NMJ innervation in G93A mice at doses of 5 ($P<0.05$), 15, and 25 mg/(kg·day) ($P<0.01$). Statistics were evaluated using 1-way ANOVA with Dunnett's post-hoc test. *$P<0.05$, **$P<0.01$.
doi:10.1371/journal.pone.0046185.g006

mice, hyperphosphorylation and upregulation of c-Abl was apparent in the lumbar spinal cord. Notably, although apoptosis-related molecules such as c-Abl were expected to exert their function at a relatively late stage of disease [34,35], the expression of c-Abl was increased at the presymptomatic stage. This unexpected result suggests that c-Abl may be an early player in the apoptotic cascade of ALS pathogenesis and thus a promising target to protect motor neurons against cytotoxic insults.

The currently available c-Abl inhibitors are imatinib, dasatinib, and nilotinib, all of which have been used for the treatment of CML, Ph+ALL, and gastrointestinal stromal tumor [36,37,38]. A number of studies have reported CNS relapse in patients treated with imatinib, which has poor BBB permeability [39,40,41,42,43,44], while in contrast, Porkka et al. reported that dasatinib crossed the BBB and showed therapeutic efficacy against CNS CML tumors in a mouse model and in patients with CNS leukemia (Ph+ALL) [45]. The high BBB permeability of dasatinib is advantageous for the treatment of ALS, since it is expected to achieve a sufficient therapeutic concentration in the CNS. We demonstrated that dasatinib at a dose of 15 mg/(kg·day) or more delayed disease progression and extended the survival of G93A mice. Immunostaining of spinal cords clearly demonstrated a dose-dependent protective effect of dasatinib on motor neuron survival by inhibiting apoptosis. These results indicate that c-Abl plays an

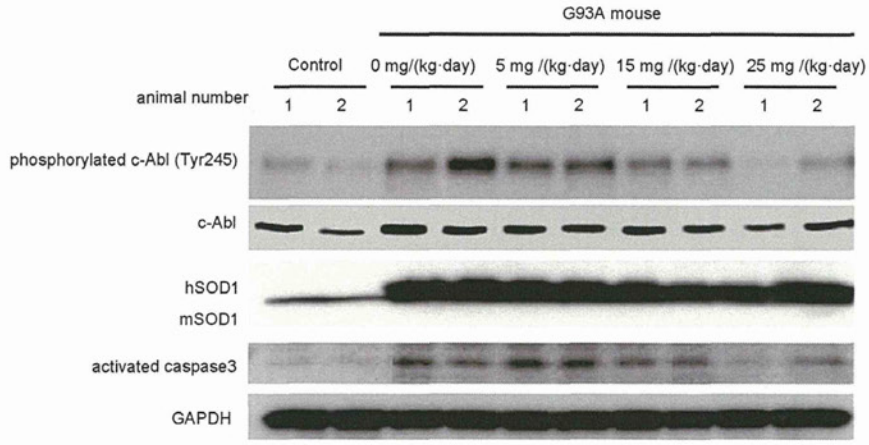

Figure 7. Dasatinib inhibits c-Abl phosphorylation in G93A mice. Protein levels of phosphorylated c-Abl (Tyr245), c-Abl, and activated caspase-3 were measured by western blot analysis using spinal cords from dasatinib- and vehicle-treated G93A mice (120 days old). GAPDH is shown as the loading control. hSOD1 and mSOD1 indicate human SOD1 and mouse endogenous SOD1, respectively. Western blot analysis is shown in duplicate. The animal number refers to individual animals. Parallel declines in c-Abl phosphorylation and activated caspase 3 were observed.
doi:10.1371/journal.pone.0046185.g007

important role in the disease pathogenesis of ALS in G93A mice and is a promising therapeutic target for ALS.

Since the involvement of c-Abl upregulation and activation has been demonstrated in neuronal cell apoptosis [46,47], we investigated whether upregulation of c-Abl is associated with an increased level of activated caspase-3, which correlates with apoptosis. Our results clearly showed that caspase 3 was activated in the spinal cords of G93A mice. Administration of dasatinib attenuated both c-Abl phosphorylation and caspase-3 activation in a dose-dependent manner. Thus, our results suggest that dasatinib ameliorates the phenotype of these animals by suppressing apoptotic cell death of motor neurons caused by mutant SOD1.

The examination of NMJs revealed that dasatinib successfully reversed the deinnervation of NMJs, an early pathological change reflecting motor neuron degeneration in mutant SOD1-mediated ALS [48]. Since levels of total and active c-Abl were increased in the spinal cords of G93A mice at the early stage of the disease (Fig. 4), dasatinib appears to improve NMJ function via c-Abl-mediated signaling. These findings suggest that dasatinib improved motor neuron function leading to amelioration of weight loss in G93A mice. They also demonstrate that the loss of synaptic contacts is a sensitive indicator of the beneficial effects exerted by dasatinib in G93A mice.

One possible explanation for the relatively small effects of dasatinib in this study is that the beneficial effects of this therapy on apoptosis were limited in motor neurons and could not reverse the physical dysfunction of the mice, despite the improvement in innervation at NMJs. Alternatively, dasatinib may not be capable of mitigating non-apoptotic pathways of motor neuron degeneration caused by mutant SOD1, since non-apoptotic programmed cell death has also been implicated in motor neuron damage in G93A mice [49]. Taken together, dasatinib may mitigate apoptotic events that occur at an early stage of the disease and partially improve motor neuron function via activation of c-Abl.

Using human postmortem spinal cord tissue, we demonstrated a significant increase in c-Abl expression in the spinal cord of sALS compared with non-ALS. Histochemical findings confirmed that c-Abl protein increased mainly in motor neurons. In addition, c-Abl phosphorylation was also increased in motor neurons in the affected area. These findings indicate that c-Abl abnormality is involved in human sALS cases as well as cellular and animal models of ALS. Thus far, not many drug candidates derived from research using mutant SOD1 transgenic animals have been successful in clinical trials for human sALS [50]. The implication of c-Abl in sALS as well as mutant SOD1-associated ALS supports the possible application of dasatinib as a candidate drug for sALS treatment. Our study showed that dasatinib treatment suppressed apoptosis and delayed disease progression in G93A mice, suggesting that dasatinib has a potential therapeutic value in humans, since apoptosis appears to be an important target of treatment development for ALS [35,51].

In conclusion, the major findings of this study are (1) the observation of c-Abl upregulation and activation in the spinal cords of G93A mice at a relatively early stage of the disease; (2) the improved survival of G93A mice with concomitant suppression of c-Abl phosphorylation and caspase-3 activation upon administration of a BBB-permeable c-Abl inhibitor, dasatinib; and (3) increased c-Abl expression and phosphorylation in postmortem spinal cord tissues from sALS patients. Taken together, our results suggest that c-Abl is a novel therapeutic target for ALS.

Materials and Methods

Cell lines

The mouse motor neuron hybridoma line NSC-34 was provided by Dr. N.R. Cashman (University of Toronto; Toronto, Canada) [30]. Human wild-type and mutant (G93A and G85R) SOD1 cDNAs were subcloned from pcDNA3.1/SOD1 into lentiviral expression vectors (pLenti-CMV/TO, kind gifts from Dr. Eric Campeau at the University of Massachusetts Medical School) [52]. Lentiviral particles were produced in HEK293T cells (Open Biosystems, Huntsville, AL, USA) by transfection with Lipofectamine 2000 (Invitrogen, Eugene, OR, USA). Lentivirus-containing supernatant was collected 48 h after transfection and stored at −80°C. Details of the lentivirus system have been described previously [52]. We first transduced the Tet repressor into NSC-34 cells and selected a single clone (NSC-34-TetR14) that demonstrated good induction without leaky expression. NSC-34-TetR14 cells were stably transduced with lentivirus-Tet-on/SOD1, an inducible lentivirus expressing Myc-tagged wild-type or mutant SOD1.

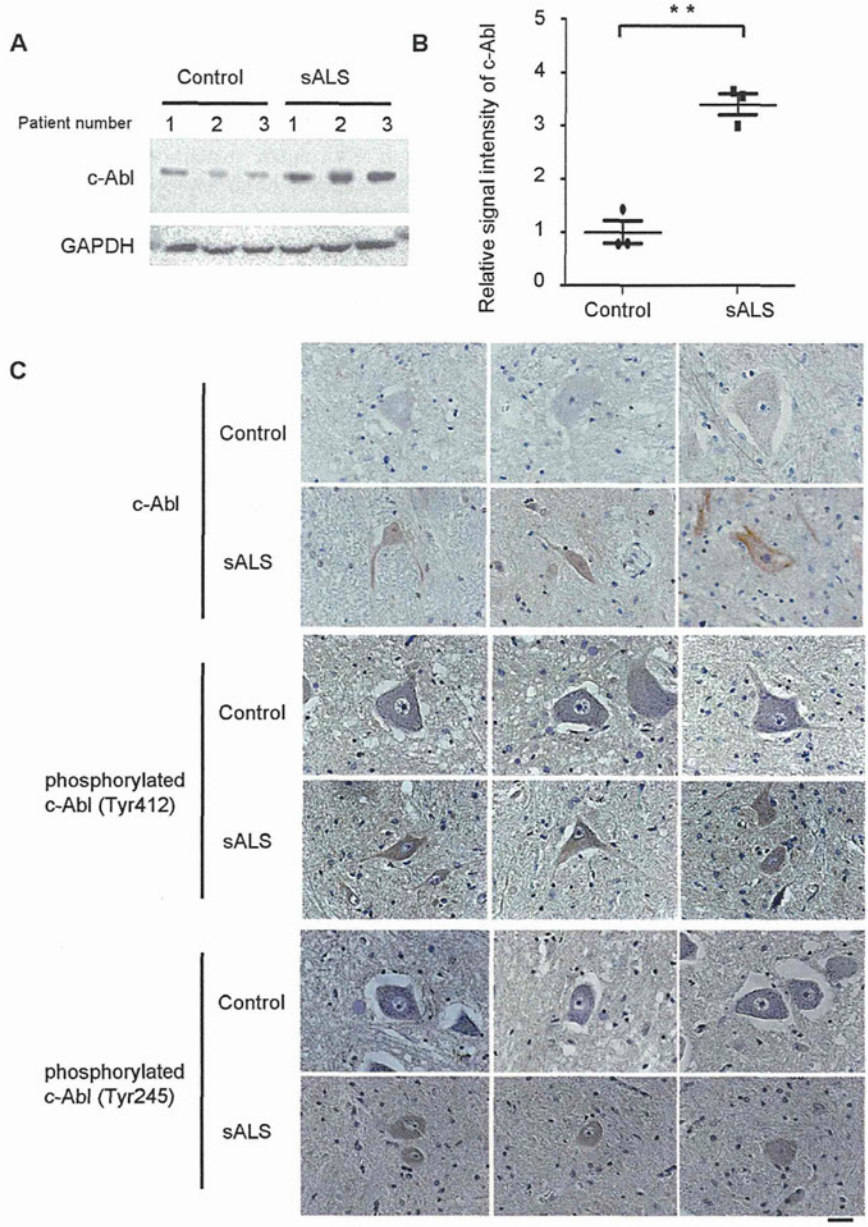

Figure 8. c-Abl upregulation and activation in affected motor neurons of sporadic ALS patients. A: The protein expression of total c-Abl was measured by western blot analysis using an anti-c-Abl antibody and the lumbar spinal cord tissue from sporadic ALS (sALS) cases and controls. GAPDH is shown as an internal control. The patient number refers to individual patients. B: Densitometric analysis using Image J software revealed a significant difference in the amount of total c-Abl protein in the lumbar spinal cords of sALS patients and controls ($P<0.01$). Data are presented as mean ± SEM. Statistical analysis was performed using Student's *t* test. $^{**}P<0.01$. C: Immunohistochemical analysis using paraffin-embedded spinal cords from control and sALS patients was carried out by staining with anti-c-Abl, anti-phosphorylated c-Abl (Tyr412), and anti-phosphorylated c-Abl (Tyr245) antibodies. Scale bar: 50 μm.
doi:10.1371/journal.pone.0046185.g008

Cell culture

NSC-34 cells were grown in Dulbecco's modified Eagle's medium (DMEM) containing 10% fetal calf serum (FCS; Invitrogen). The tet-on inducible cell lines were grown in DMEM supplemented with 10% tetracycline-free FCS (Clontech, Mountain View, CA, USA). All cell lines used in this study were cultured at 37°C in an atmosphere of 5% CO_2. We induced hSOD1 expression by adding 2 μg/ml doxycycline (Clontech) to the culture medium for the last 48 h of culture.

Cell viability assay

Each of the cell lines (3,500 cells per well) were grown on collagen-coated 96-well plates with serum-free medium. MTS (3-(4,5-dimethylthiazol-2-yl)-5-(3-carboxymethoxyphenyl)-2-(4-sulfophenyl)-2H-tetrazolium)-based cell proliferation assays were performed after 48 h of induction with doxycycline (Dox, 2 μg/ml) using the CellTiter 96® AQueous One Solution Cell Proliferation Assay (Promega, Madison, WI, USA). Briefly, we added CellTiter 96® AQueous One Solution Reagent to each well of a 96-well assay plate containing the samples in culture medium. After incubation at 37°C for 1 h, absorbance at 490 nm was measured

using a multiple-plate reader (Powerscan HT, Dainippon Pharmaceutical, Osaka, Japan), with assays carried out in triplicate.

Cytotoxicity detection assay

Cell injury was quantitatively assessed by measurement of LDH released from damaged or destroyed cells into the extracellular fluid after 48-h induction of wild-type or mutant SOD1. The activity of LDH released into the culture medium was measured with a Cytotoxicity Detection kit (Roche Applied Science, Burgess Hill, UK) according to the manufacturer's protocol. Briefly, after 48 h of induction with doxycycline (Dox, 2 μg/ml), we added substrate mixture from the kit to each well of a 96-well assay plate containing the culture supernatant. Following incubation for 30 min, absorbance at 490 nm was measured using a multiple-plate reader (Powerscan HT, Dainippon Pharmaceutical, Osaka, Japan).

Transgenic mice

Transgenic mice overexpressing the human SOD1 gene carrying the G93A mutation were purchased from the Jackson Laboratory (Bar Harbor, ME, USA) and maintained as hemizygotes by mating transgenic males with B6/SJLF1 females [53]. All animal experiments were performed in accordance with the National Institute of Health Guide for the Care and Use of Laboratory Animals and were approved by the Nagoya University Animal Experiment Committee.

Chemicals

Dasatinib was provided by Bristol-Myers Squibb. Propylene glycol was purchased from Sigma Chemical Co. (St Louis, MO, USA). SU6656 was purchased from Calbiochem (Darmstadt, Germany). All other chemicals used were reagent grade or better.

Drug formulation and administration

For oral administration, dasatinib was dissolved in a mixture of propylene glycol/water (50:50). The administration volume was 0.01 ml/g. Ludolph et al. recommended that a total of 48 G93A mice should be used in a preclinical trial if 2 groups (treated animals and controls; $n = 24$ per group) are to be compared, and recommended that the number of animals should be increased for testing the dose-response effect of a drug [50]. Therefore, we allocated 28 mice to each treatment group for the survival analysis. From postnatal day 56, dasatinib was administered by oral gavage using a 5-days-on/2-days-off once-daily schedule (Monday through Friday) at doses of 5, 15, and 25 mg/(kg·day). Control mice received vehicle alone.

Immunohistochemistry

Under pentobarbital anesthesia, mice were transcardially perfused with 20 ml phosphate buffer (pH 7.4). Tissues were postfixed overnight in 10% phosphate-buffered formalin and processed for paraffin embedding as previously described [54]. Transverse sections of spinal cord (6-μm thickness) were then deparaffinized with alcohol, rehydrated, and microwaved in 0.1 M citrate buffer (pH 6) as a pretreatment for antigen retrieval. Immunostaining was performed using the EnVision+ System-HRP (Dako, Glostrup, Denmark). Tissue sections were incubated with anti-c-Abl antibody (Abcam, Cambridge, MA) and anti-phospho-c-Abl (Tyr412 or Tyr245) antibody (Cell Signaling Technology, Beverly, MA, USA), both diluted 1:100 in Dako antibody diluent (Dako) for immunohistochemical analysis. Counterstaining was performed using hematoxylin. For fluorescence microscopic analysis, after antigen retrieval, tissue sections were incubated with TNB-buffer (0.10 M Tris-HCl, 0.15 M NaCl, 0.5% BMP) for 30 min at room temperature to block non-specific antibody binding. Then spinal tissue sections were incubated with anti-phospho-c-Abl (Tyr412 or Tyr245) antibody (Cell Signaling Technology), both diluted 1:100 in phosphate buffered saline (PBS) buffer, overnight at 4°C. After incubation with primary antibody, the sections were exposed to an appropriate secondary antibody conjugated to fluorescent dye and Topro-3 (Invitrogen) for 1 h at room temperature. Sections were visualized using a confocal microscope (LSM 710, Carl Zeiss, Oberkochen, Germany) under epifluorescent illumination. The intensity of immunostained neurons was semi-quantified using NIH Image J software (v 1.44, NIH, Bethesda, MD, USA).

Assessment of motor function

The motor performance of mice was assessed weekly using an Economex Rotarod (Columbus Instruments, Columbus, OH, USA) starting at 42 days of age. Staying on the rod for more than 180 s was considered to be the normal performance level, as previously described [55].

Western blot analyses

The spinal cords of dasatinib- and vehicle-treated mice were collected approximately 3 h after the final oral administration. Human and mouse spinal cords were snap frozen in liquid nitrogen, homogenized in ice-cold Cell Lytic-M Mammalian Cell Lysis/Extraction Reagent (Sigma), and centrifuged at $18,800 \times g$ for 15 min at 4°C. Protein concentration was determined by DC protein assay (Bio-Rad, Hercules, CA, USA). Western blotting was performed using standard procedures as described previously [56,57]. Primary antibodies were used at the following concentrations: anti-SOD1, 1:2,000 (Abcam); anti-Myc, 1:1,000 (MBL, Nagoya, Japan); anti-tubulin, 1:1,000 (Sigma); anti-c-Abl, 1:1,000 (BD Transduction); anti-phospho-c-Abl (Tyr412), 1:1,000 (Sigma); anti-phospho-c-Abl (Tyr245), 1:1000 (Cell Signaling Technology); anti-glyceraldehyde-3-phosphate dehydrogenase (GAPDH), 1:1,000 (Millipore, Billerica, MA); anti-phospho-c-Src (Tyr416), 1:1,000 (Cell Signaling Technology); anti c-Src, 1:1,000 (Cell Signaling Technology); and anti-cleaved caspase-3 (Asp175), 1:1,000 (Cell Signaling Technology). Secondary antibody probing and detection were performed using the ECL Plus kit (GE Healthcare, Buckinghamshire, UK). For detection of phosphorylated c-Abl, antibody was diluted in Tris-buffered saline (TBS) with Tween (0.5%) containing 3% BSA, otherwise 5% fat-free milk in TBS with Tween (0.5%) was used as the antibody dilutant. Chemiluminescence signals were digitalized (LAS-3000 Imaging System; Fujifilm, Tokyo, Japan), and band intensities were quantified using Multi Gauge software version 3.0 (Fujifilm).

Quantitative real-time PCR

Real-time PCR was performed as described previously [58]. In brief, total RNA from either mouse spinal cord or NSC-34 cells was reverse transcribed into first-strand cDNA using SuperScript II reverse transcriptase (Invitrogen). Real-time PCR was performed using QuantiTect SYBR Green PCR Master Mix and 0.4 M of each primer (Qiagen, Valencia, CA, USA), and the product was detected using the CFX96™ real-time system (Bio-Rad Laboratories). The reaction conditions were 95°C for 15 min, followed by 40 cycles of 15 s at 94°C, 30 s at 55°C, and 30 s at 72°C. The expression level of GAPDH was quantified and used as an internal standard control. The primers used were 5′-TCGTTACCTCCAAAGGCTGCTC-3′ and 5′-ATGGCGGTGTCTGGCTATTCA-3′ for c-Abl and 5′-TCAA-

GAAGGTGGTGAAGCAG-3′ and 5′-GTTGAAGTCGCAG-GAGACAA-3′ for GAPDH.

Motor neuron assessment by immunohistochemical analysis

At age 120 days, 8 animals from each treatment group were sacrificed, and the lumbar spinal cords (L1-3) were collected. The samples were embedded in paraffin, and 6-μm sections were prepared. Spinal cord tissue sections were immunostained with anti-ChAT antibody (Millipore) diluted 1:1,000 in Dako antibody diluent (Dako) using the EnVision+ System-HRP (Dako). ChAT-immunoreactive neurons in the ventral horn of the lumbar spinal cord (L1–3) were counted in 3 sections taken at 60-μm intervals, and the mean total number of ChAT-immunoreactive neurons was compared between treatment groups. The area (pixels) of ChAT-immunoreactive neurons was analyzed using NIH Image J software (NIH). ChAT-positive cells with an area greater than 100 μm^2 were presumed to be motor neurons.

NMJ assessment by immunohistochemical analysis

At the age of 120 days, 8 animals from each treatment group were sacrificed, and quadriceps femoris specimens were quickly frozen in liquid nitrogen. The samples were mounted in Tissue-Tek OCT compound (Sakura, Tokyo, Japan), and 30-μm cryostat sections were prepared from the frozen tissues. Frozen sections were fixed in acetone for 5 min and then incubated with TNB-buffer (0.10 M Tris-HCl, 0.15 M NaCl, 0.5% BMP) for 15 min at room temperature to block non-specific antibody binding. Sections were incubated with primary antibodies and alpha-BuTX overnight at 4°C. The following primary antibodies were used: anti-synaptophysin diluted 1:100 (Cell Signaling Technology) and anti-SMI31, 1:100 (COVANCE, Princeton, NJ, USA). Alpha-BuTX biotin-XX-conjugate diluted 1:80 was purchased from Molecular Probes (Eugene, OR, USA). After washing with PBS, the sections were exposed to appropriate secondary antibody and streptavidin-conjugated fluorescent dye for 1 h at room temperature, then washed with PBS again and mounted. Sections were examined and photographed using a confocal microscope (LSM 710, Carl Zeiss) under epifluorescent illumination.

Human sporadic ALS samples

Spinal cord specimens were obtained at autopsy from 3 pathologically confirmed cases of sALS (2 men, aged 71 and 73 y, and 1 woman, aged 53 y) and 3 cases of non-neurodegenerative disease. Lumbar spinal cord tissue was either homogenized for western blot analysis or embedded in paraffin for immunohistochemical analysis. The collection of autopsied human tissues and their use for this study were approved by the Ethics Committee of Nagoya University Graduate School of Medicine, and written informed consent was obtained from the patients' next-of-kin. Experimental procedures involving human subjects were conducted in conformance with the principles expressed in the Declaration of Helsinki.

Statistical analyses

Statistical analyses were performed using Prism software (GraphPad Software, La Jolla, CA, USA). Biochemical data were statistically analyzed using Student's t test or 1-factor factorial ANOVA followed by appropriate post-hoc tests. Survival data was analyzed by log-rank tests, and body weight change was analyzed by 2-factor factorial ANOVA. P values of 0.05 or less were considered to be statistically significant.

Supporting Information

Figure S1 Increased phosphorylated c-Abl in spinal cords of G93A mice. A: The distribution of phosphorylated c-Abl proteins was analyzed by immunohistochemical staining of paraffin-embedded spinal cord sections from G93A mice (10, 14, and 18 weeks old) and control littermates (20 weeks old) using antibodies directed against phosphorylated c-Abl (Tyr245 and Tyr412). The spinal sections were immunostained with anti-ChAT (red) and anti-phosphorylated c-Abl (Tyr245 or Tyr412) (green) antibodies together with Topro-3 (blue). Representative immunostained motor neurons visualized with confocal laser scanning microscopy are shown. Scale bar: 50 μm. B: The intensity of motor neurons labeled with anti-phosphorylated c-Abl (Tyr245) and anti-phosphorylated c-Abl (Tyr412) antibodies shown in A was quantified (n = 3 mice per group). Phosphorylated c-Abl immunoreactivity with both antibodies was significantly increased in the spinal cords of G93A mice ($P<0.01$). The value was standardized to that of the fluorescence intensity of control mice. Statistics were evaluated using 1-way ANOVA with Dunnett's post-hoc test. $^{**}P<0.01$.
(TIF)

Figure S2 Dasatinib reduced c-Abl phosphorylation (Tyr412) in G93A mice. A: Phosphorylated c-Abl (Tyr412) protein was analyzed by immunohistochemical staining of paraffin-embedded spinal cord sections from dasatinib-treated G93A mice (0, 5, 15, and 25 mg/(kg·day)) using an antibody against phosphorylated c-Abl (Tyr412). The spinal sections were fluorescently immunostained with anti-ChAT (red) and anti-phosphorylated c-Abl (Tyr412) (green) antibodies together with Topro-3 (blue). Representative immunostained motor neurons visualized with confocal laser scanning microscopy are shown. Scale bar: 50 μm. B: The intensity of the cells stained with anti-phosphorylated c-Abl (Tyr412) was quantified. The mice were administered the indicated amounts of dasatinib daily from postnatal day 56 to day 120 (n = 3 mice per group). Immunoreactivity against phosphorylated c-Abl (Tyr412) was significantly decreased in dasatinib-treated G93A mice (15 mg/(kg·day) or more) compared to vehicle-treated G93A mice ($P<0.01$, 15 mg/(kg·day) and 25 mg/(kg·day)). The value was standardized to that of the fluorescence intensity of vehicle-treated G93A mice. Statistics were evaluated using 1-way ANOVA with Dunnett's post-hoc test. $^{**}P<0.01$.
(TIF)

Acknowledgments

NSC-34 cells were kindly provided by Dr. N. Cashman. We thank Dr. E. Campeau for providing lentiviral expression systems.

Author Contributions

Conceived and designed the experiments: RK GS. Performed the experiments: RK SI MK KK JS. Analyzed the data: RK SI MK KK JS. Contributed reagents/materials/analysis tools: RK SI MK KK ZH JS HA FT FU. Wrote the paper: RK SI MK GS.

References

1. Tyler HR, Shefner J (1991) Amyotrophic lateral sclerosis. In: Vinken PJ, Bruyn GW, Klawans HL, editors. Handbook of Clinical Neurology. Amsterdam: Elsevier Science Publishers BV. pp. 169–215.
2. Emery A, Holloway S (1982) Familial motor neuron diseases. In: Rowland L, editor. Human Motor Neuron Diseases. New York: Raven Press Ltd. pp. 139–147.
3. Rosen DR, Siddique T, Patterson D, Figlewicz DA, Sapp P, et al. (1993) Mutations in Cu/Zn superoxide dismutase gene are associated with familial amyotrophic lateral sclerosis. Nature 362: 59–62.
4. Martin LJ, Liu Z, Chen K, Price AC, Pan Y, et al. (2007) Motor neuron degeneration in amyotrophic lateral sclerosis mutant superoxide dismutase-1 transgenic mice: mechanisms of mitochondriopathy and cell death. J Comp Neurol 500: 20–46.
5. Bruijn LI, Houseweart MK, Kato S, Anderson KL, Anderson SD, et al. (1998) Aggregation and motor neuron toxicity of an ALS-linked SOD1 mutant independent from wild-type SOD1. Science 281: 1851–1854.
6. Boillee S, Vande Velde C, Cleveland DW (2006) ALS: a disease of motor neurons and their nonneuronal neighbors. Neuron 52: 39–59.
7. Julien JP (2001) Amyotrophic lateral sclerosis. unfolding the toxicity of the misfolded. Cell 104: 581–591.
8. Kabashi E, Durham HD (2006) Failure of protein quality control in amyotrophic lateral sclerosis. Biochim Biophys Acta 1762: 1038–1050.
9. Cassina P, Cassina A, Pehar M, Castellanos R, Gandelman M, et al. (2008) Mitochondrial dysfunction in SOD1G93A-bearing astrocytes promotes motor neuron degeneration: prevention by mitochondrial-targeted antioxidants. J Neurosci 28: 4115–4122.
10. Jiang YM, Yamamoto M, Kobayashi Y, Yoshihara T, Liang Y, et al. (2005) Gene expression profile of spinal motor neurons in sporadic amyotrophic lateral sclerosis. Ann Neurol 57: 236–251.
11. Jiang YM, Yamamoto M, Tanaka F, Ishigaki S, Katsuno M, et al. (2007) Gene expressions specifically detected in motor neurons (dynactin 1, early growth response 3, acetyl-CoA transporter, death receptor 5, and cyclin C) differentially correlate to pathologic markers in sporadic amyotrophic lateral sclerosis. J Neuropathol Exp Neurol 66: 617–627.
12. Wang JY, Ledley F, Goff S, Lee R, Groner Y, et al. (1984) The mouse c-abl locus: molecular cloning and characterization. Cell 36: 349–356.
13. Nowell PC, Hungerford DA (1960) A minute chromosome in human chronic granulocytic leukemia. Science 132: 1488–1501.
14. Fainstein E, Marcelle C, Rosner A, Canaani E, Gale RP, et al. (1987) A new fused transcript in Philadelphia chromosome positive acute lymphocytic leukaemia. Nature 330: 386–388.
15. Brasher BB, Van Etten RA (2000) c-Abl has high intrinsic tyrosine kinase activity that is stimulated by mutation of the Src homology 3 domain and by autophosphorylation at two distinct regulatory tyrosines. J Biol Chem 275: 35631–35637.
16. Sirvent A, Benistant C, Roche S (2008) Cytoplasmic signalling by the c-Abl tyrosine kinase in normal and cancer cells. Biol Cell 100: 617–631.
17. Pendergast AM (2002) The Abl family kinases: mechanisms of regulation and signaling. Adv Cancer Res 85: 51–100.
18. Zandy NL, Playford M, Pendergast AM (2007) Abl tyrosine kinases regulate cell-cell adhesion through Rho GTPases. Proc Natl Acad Sci U S A 104: 17686–17691.
19. Gu JJ, Ryu JR, Pendergast AM (2009) Abl tyrosine kinases in T-cell signaling. Immunol Rev 228: 170–183.
20. Wang JY (2000) Regulation of cell death by the Abl tyrosine kinase. Oncogene 19: 5643–5650.
21. Yuan ZM, Shioya H, Ishiko T, Sun X, Gu J, et al. (1999) p73 is regulated by tyrosine kinase c-Abl in the apoptotic response to DNA damage. Nature 399: 814–817.
22. Wang JY, Ki SW (2001) Choosing between growth arrest and apoptosis through the retinoblastoma tumour suppressor protein, Abl and p73. Biochem Soc Trans 29: 666–673.
23. Lu W, Finnis S, Xiang C, Lee HK, Markowitz Y, et al. (2007) Tyrosine 311 is phosphorylated by c-Abl and promotes the apoptotic effect of PKCdelta in glioma cells. Biochem Biophys Res Commun 352: 431–436.
24. Chen TC, Lai YK, Yu CK, Juang JL (2007) Enterovirus 71 triggering of neuronal apoptosis through activation of Abl-Cdk5 signalling. Cell Microbiol 9: 2676–2688.
25. Lee JH, Jeong MW, Kim W, Choi YH, Kim KT (2008) Cooperative roles of c-Abl and Cdk5 in regulation of p53 in response to oxidative stress. J Biol Chem 283: 19826–19835.
26. Zukerberg LR, Patrick GN, Nikolic M, Humbert S, Wu CL, et al. (2000) Cables links Cdk5 and c-Abl and facilitates Cdk5 tyrosine phosphorylation, kinase upregulation, and neurite outgrowth. Neuron 26: 633–646.
27. Koleske AJ, Gifford AM, Scott ML, Nee M, Bronson RT, et al. (1998) Essential roles for the Abl and Arg tyrosine kinases in neurulation. Neuron 21: 1259–1272.
28. Cancino GI, Toledo EM, Leal NR, Hernandez DE, Yevenes LF, et al. (2008) STI571 prevents apoptosis, tau phosphorylation and behavioural impairments induced by Alzheimer's beta-amyloid deposits. Brain 131: 2425–2442.
29. Alvarez AR, Sandoval PC, Leal NR, Castro PU, Kosik KS (2004) Activation of the neuronal c-Abl tyrosine kinase by amyloid-beta-peptide and reactive oxygen species. Neurobiol Dis 17: 326–336.
30. Cashman NR, Durham HD, Blusztajn JK, Oda K, Tabira T, et al. (1992) Neuroblastoma x spinal cord (NSC) hybrid cell lines resemble developing motor neurons. Dev Dyn 194: 209–221.
31. Lombardo LJ, Lee FY, Chen P, Norris D, Barrish JC, et al. (2004) Discovery of N-(2-chloro-6-methyl- phenyl)-2-(6-(4-(2-hydroxyethyl)- piperazin-1-yl)-2-methylpyrimidin-4-ylamino)thiazole-5-carboxamide (BMS-354825), a dual Src/Abl kinase inhibitor with potent antitumor activity in preclinical assays. J Med Chem 47: 6658–6661.
32. Blake RA, Broome MA, Liu X, Wu J, Gishizky M, et al. (2000) SU6656, a selective src family kinase inhibitor, used to probe growth factor signaling. Mol Cell Biol 20: 9018–9027.
33. Alvarez AR, Klein A, Castro J, Cancino GI, Amigo J, et al. (2008) Imatinib therapy blocks cerebellar apoptosis and improves neurological symptoms in a mouse model of Niemann-Pick type C disease. FASEB J 22: 3617–3627.
34. Dangond F, Hwang D, Camelo S, Pasinelli P, Frosch MP, et al. (2004) Molecular signature of late-stage human ALS revealed by expression profiling of postmortem spinal cord gray matter. Physiol Genomics 16: 229–239.
35. Martin LJ (2010) Mitochondrial and cell death mechanisms in neurodegenerative diseases. Pharmaceuticals (Basel) 3: 839–915.
36. An X, Tiwari AK, Sun Y, Ding PR, Ashby CR, Jr., et al. (2010) BCR-ABL tyrosine kinase inhibitors in the treatment of Philadelphia chromosome positive chronic myeloid leukemia: a review. Leuk Res 34: 1255–1268.
37. Agrawal M, Garg RJ, Kantarjian H, Cortes J (2010) Chronic myeloid leukemia in the tyrosine kinase inhibitor era: what is the "best" therapy? Curr Oncol Rep 12: 302–313.
38. Braconi C, Bracci R, Cellerino R (2008) Molecular targets in Gastrointestinal Stromal Tumors (GIST) therapy. Curr Cancer Drug Targets 8: 359–366.
39. Isobe Y, Sugimoto K, Masuda A, Hamano Y, Oshimi K (2009) Central nervous system is a sanctuary site for chronic myelogenous leukaemia treated with imatinib mesylate. Intern Med J 39: 408–411.
40. Aichberger KJ, Herndlhofer S, Agis H, Sperr WR, Esterbauer H, et al. (2007) Liposomal cytarabine for treatment of myeloid central nervous system relapse in chronic myeloid leukaemia occurring during imatinib therapy. Eur J Clin Invest 37: 808–813.
41. Simpson E, O'Brien SG, Reilly JT (2006) Extramedullary blast crises in CML patients in complete hematological remission treated with imatinib mesylate. Clin Lab Haematol 28: 215–216.
42. Matsuda M, Morita Y, Shimada T, Miyatake J, Hirase C, et al. (2005) Extramedullary blast crisis derived from 2 different clones in the central nervous system and neck during complete cytogenetic remission of chronic myelogenous leukemia treated with imatinib mesylate. Int J Hematol 81: 307–309.
43. Rajappa S, Uppin SG, Raghunadharao D, Rao IS, Surath A (2004) Isolated central nervous system blast crisis in chronic myeloid leukemia. Hematol Oncol 22: 179–181.
44. Bujassoum S, Rifkind J, Lipton JH (2004) Isolated central nervous system relapse in lymphoid blast crisis chronic myeloid leukemia and acute lymphoblastic leukemia in patients on imatinib therapy. Leuk Lymphoma 45: 401–403.
45. Porkka K, Koskenvesa P, Lundan T, Rimpilainen J, Mustjoki S, et al. (2008) Dasatinib crosses the blood-brain barrier and is an efficient therapy for central nervous system Philadelphia chromosome-positive leukemia. Blood 112: 1005–1012.
46. Ito Y, Pandey P, Mishra N, Kumar S, Narula N, et al. (2001) Targeting of the c-Abl tyrosine kinase to mitochondria in endoplasmic reticulum stress-induced apoptosis. Mol Cell Biol 21: 6233–6242.
47. Gonfloni S (2010) DNA damage stress response in germ cells: role of c-Abl and clinical implications. Oncogene 29: 6193–6202.
48. Kanning KC, Kaplan A, Henderson CE (2010) Motor neuron diversity in development and disease. Annu Rev Neurosci 33: 409–440.
49. Vila M, Przedborski S (2003) Targeting programmed cell death in neurodegenerative diseases. Nat Rev Neurosci 4: 365–375.
50. Ludolph AC, Bendotti C, Blaugrund E, Hengerer B, Loffler JP, et al. (2007) Guidelines for the preclinical in vivo evaluation of pharmacological active drugs for ALS/MND: report on the 142nd ENMC international workshop. Amyotroph Lateral Scler 8: 217–223.
51. Inoue H, Tsukita K, Iwasato T, Suzuki Y, Tomioka M, et al. (2003) The crucial role of caspase-9 in the disease progression of a transgenic ALS mouse model. EMBO J 22: 6665–6674.
52. Campeau E, Ruhl VE, Rodier F, Smith CL, Rahmberg BL, et al. (2009) A versatile viral system for expression and depletion of proteins in mammalian cells. PLoS One 4: e6529.
53. Gurney ME, Pu H, Chiu AY, Dal Canto MC, Polchow CY, et al. (1994) Motor neuron degeneration in mice that express a human Cu,Zn superoxide dismutase mutation. Science 264: 1772–1775.
54. Adachi H, Kume A, Li M, Nakagomi Y, Niwa H, et al. (2001) Transgenic mice with an expanded CAG repeat controlled by the human AR promoter show polyglutamine nuclear inclusions and neuronal dysfunction without neuronal cell death. Hum Mol Genet 10: 1039–1048.

55. Adachi H, Waza M, Tokui K, Katsuno M, Minamiyama M, et al. (2007) CHIP overexpression reduces mutant androgen receptor protein and ameliorates phenotypes of the spinal and bulbar muscular atrophy transgenic mouse model. J Neurosci 27: 5115–5126.
56. Minamiyama M, Katsuno M, Adachi H, Waza M, Sang C, et al. (2004) Sodium butyrate ameliorates phenotypic expression in a transgenic mouse model of spinal and bulbar muscular atrophy. Hum Mol Genet 13: 1183–1192.
57. Katsuno M, Adachi H, Kume A, Li M, Nakagomi Y, et al. (2002) Testosterone reduction prevents phenotypic expression in a transgenic mouse model of spinal and bulbar muscular atrophy. Neuron 35: 843–854.
58. Ishigaki S, Liang Y, Yamamoto M, Niwa J, Ando Y, et al. (2002) X-Linked inhibitor of apoptosis protein is involved in mutant SOD1-mediated neuronal degeneration. J Neurochem 82: 576–584.

REPORT

The TRK-Fused Gene Is Mutated in Hereditary Motor and Sensory Neuropathy with Proximal Dominant Involvement

Hiroyuki Ishiura,[1] Wataru Sako,[3] Mari Yoshida,[4] Toshitaka Kawarai,[3] Osamu Tanabe,[3,5] Jun Goto,[1] Yuji Takahashi,[1] Hidetoshi Date,[1] Jun Mitsui,[1] Budrul Ahsan,[1] Yaeko Ichikawa,[1] Atsushi Iwata,[1] Hiide Yoshino,[6] Yuishin Izumi,[3] Koji Fujita,[3] Kouji Maeda,[3] Satoshi Goto,[3] Hidetaka Koizumi,[3] Ryoma Morigaki,[3] Masako Ikemura,[7] Naoko Yamauchi,[7] Shigeo Murayama,[8] Garth A. Nicholson,[9] Hidefumi Ito,[10] Gen Sobue,[11] Masanori Nakagawa,[12] Ryuji Kaji,[3,*] and Shoji Tsuji[1,2,13,*]

Hereditary motor and sensory neuropathy with proximal dominant involvement (HMSN-P) is an autosomal-dominant neurodegenerative disorder characterized by widespread fasciculations, proximal-predominant muscle weakness, and atrophy followed by distal sensory involvement. To date, large families affected by HMSN-P have been reported from two different regions in Japan. Linkage and haplotype analyses of two previously reported families and two new families with the use of high-density SNP arrays further defined the minimum candidate region of 3.3 Mb in chromosomal region 3q12. Exome sequencing showed an identical c.854C>T (p.Pro285-Leu) mutation in the TRK-fused gene (*TFG*) in the four families. Detailed haplotype analysis suggested two independent origins of the mutation. Pathological studies of an autopsied patient revealed TFG- and ubiquitin-immunopositive cytoplasmic inclusions in the spinal and cortical motor neurons. Fragmentation of the Golgi apparatus, a frequent finding in amyotrophic lateral sclerosis, was also observed in the motor neurons with inclusion bodies. Moreover, TAR DNA-binding protein 43 kDa (TDP-43)-positive cytoplasmic inclusions were also demonstrated. In cultured cells expressing mutant TFG, cytoplasmic aggregation of TDP-43 was demonstrated. These findings indicate that formation of TFG-containing cytoplasmic inclusions and concomitant mislocalization of TDP-43 underlie motor neuron degeneration in HMSN-P. Pathological overlap of proteinopathies involving TFG and TDP-43 highlights a new pathway leading to motor neuron degeneration.

Hereditary motor and sensory neuropathy with proximal dominant involvement (HMSN-P [MIM 604484]) is an autosomal-dominant disease characterized by predominantly proximal muscle weakness and atrophy followed by distal sensory disturbances.[1] HMSN-P was first described in patients from the Okinawa Islands of Japan, where more than 100 people are estimated to be affected.[2] Two Brazilian HMSN-P-affected families of Okinawan ancestry have also been reported.[3,4]

The disease onset is usually in the 40s and is followed by a slowly progressive course. Painful muscle cramps and abundant fasciculations are observed, particularly in the early stage of the disease. In contrast to the clinical presentations of other hereditary motor and sensory neuropathies (HMSNs) presenting with predominantly distal motor weakness reflecting axonal-length dependence, the clinical presentation of HMSN-P is unique in that it involves proximal predominant weakness with widespread fasciculations resembling those of amyotrophic lateral sclerosis (ALS).[5] Distal sensory loss is accompanied later in the disease course, but the degree of the sensory involvement varies among patients. Neuropathological findings revealed severe neuronal loss and gliosis in the spinal anterior horns and mild neuronal loss and gliosis in the hypoglossal and facial nuclei of the brainstem, which indicates that the primary pathological feature of HMSN-P is a motor neuronopathy involving motor neurons, but not a motor neuropathy involving axons.[1,5] The posterior column, corticospinal tract, and spinocerebellar tract showed loss of myelinated fibers and gliosis. Neuronal loss and gliosis were found in Clarke's nucleus. Dorsal root ganglia showed mild to marked neuronal loss.[1,5] These observations suggest that HMSN-P shares neuropathological findings in part with those observed in familial ALS.[6]

Previous studies on Okinawan kindreds mapped the disease locus to chromosome 3q.[1] Subsequently, we identified two large families (families 1 and 2 in Figure 1A) affected by quite a similar phenotype in the Kansai area of Japan, located in the middle of the main island of Japan and far distant from the Okinawa Islands. We mapped the

[1]Department of Neurology, The University of Tokyo Graduate School of Medicine, 7-3-1 Hongo, Bunkyo-ku, Tokyo 113-8655, Japan; [2]Medical Genome Center, The University of Tokyo Hospital, 7-3-1 Hongo, Bunkyo-ku, Tokyo 113-8655, Japan; [3]Department of Clinical Neuroscience, The Tokushima University Graduate School of Medicine, 3-18-15 Kuramoto-cho, Tokushima 770-8503, Japan; [4]Department of Neuropathology, Institute for Medical Science of Aging, Aichi Medical University, 21 Karimata, Iwasaku, Nagakute-shi, Aichi 480-1195, Japan; [5]Department of Cell and Developmental Biology, University of Michigan Medical School, 109 Zina Pitcher Place, Ann Arbor, MI 48109-2200, USA; [6]Yoshino Neurology Clinic, 3-3-16 Konodai, Ichikawa, Chiba 272-0827, Japan; [7]Department of Pathology, Graduate School of Medicine, The University of Tokyo, 7-3-1 Hongo, Bunkyo-ku, Tokyo 113-8655, Japan; [8]Department of Neuropathology and the Brain Bank for Aging Research, Tokyo Metropolitan Institute of Gerontology, 35-2 Sakae-cho, Itabashi-ku, Tokyo 173-0015, Japan; [9]Molecular Medicine Laboratory and ANZAC Research Institute, University of Sydney, Sydney NSW 2139, Australia; [10]Department of Neurology, Kyoto University Graduate School of Medicine, 54 Kawahara-cho, Shogoin, Sakyo-ku, Kyoto 606-8507, Japan; [11]Department of Neurology, Nagoya University Graduate School of Medicine, 65 Tsurumai-cho, Showa-ku, Nagoya-shi, Aichi 466-0065, Japan; [12]Department of Neurology and Gerontology, Kyoto Prefectural University Graduate School of Medicine, 465, Kajii-cho, Kamigyo-ku, Kyoto 602-0841, Japan; [13]Division of Applied Genetics, National Institute of Genetics, Yata 1111, Mishima, Shizuoka 11-8540, Japan
*Correspondence: tsuji@m.u-tokyo.ac.jp (S.T.), rkaji@clin.med.tokushima-u.ac.jp (R.K.)
http://dx.doi.org/10.1016/j.ajhg.2012.07.014.

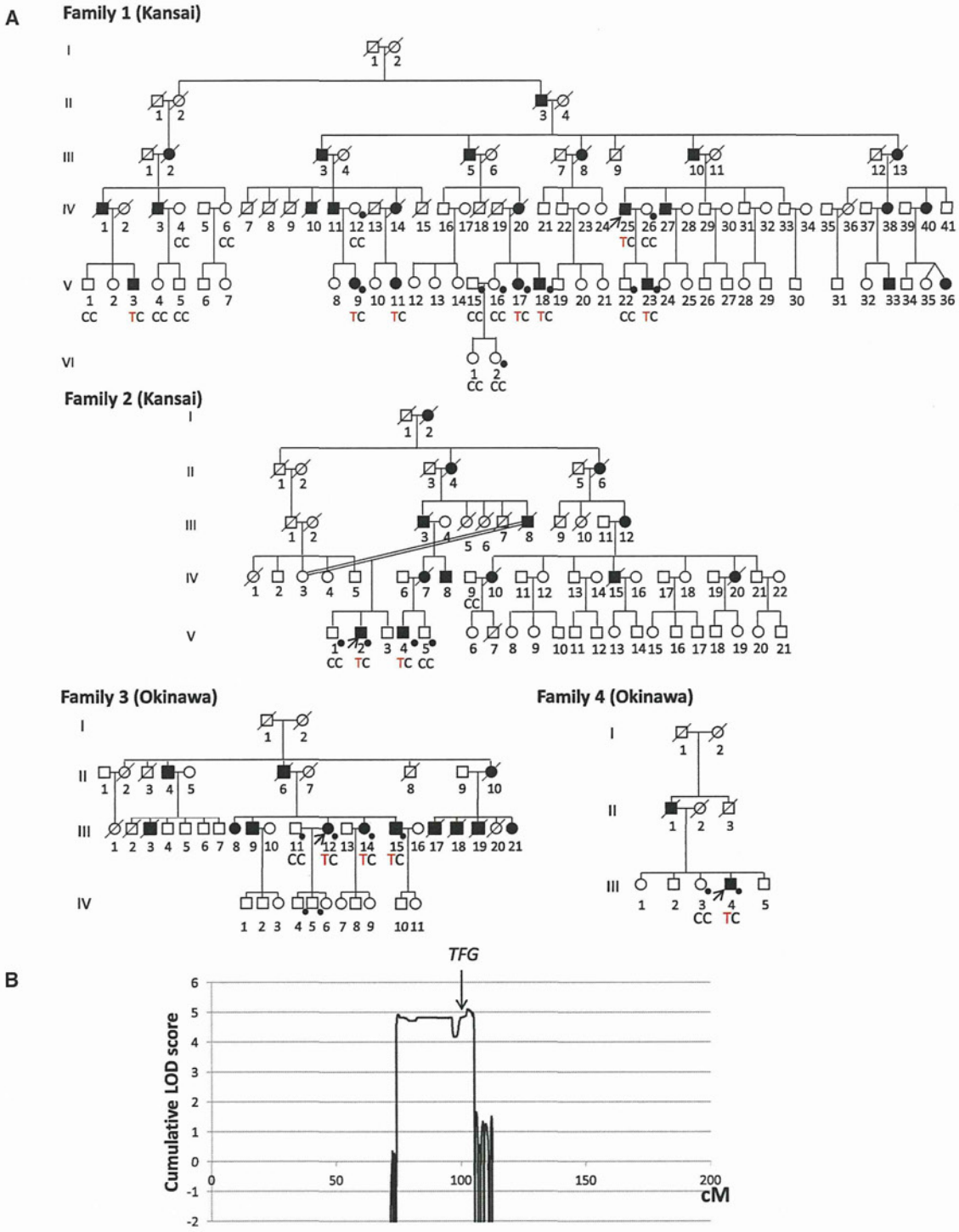

Figure 1. Pedigree Charts and Linkage Analysis

(A) Pedigree charts of families 1 and 2 (Kansai kindreds) and families 3 and 4 (Okinawan kindreds) are shown. Squares and circles indicate males and females, respectively. Affected persons are designated with filled symbols. A diagonal line through a symbol represents a deceased person. A person with an arrow is an index patient. Genotypes of *TFG* c.854 are shown in individuals in whom genomic DNA was analyzed. Individuals genotyped with SNP arrays for linkage analysis and haplotype reconstruction are indicated by dots. (B) Cumulative parametric multipoint LOD scores on chromosome 3 of all the families are shown.

disease locus to chromosome 3q,[7] overlapping with the previously defined locus, which strongly indicates that these diseases are indeed identical.

In addition to the large Kansai HMSN-P-affected families, we found two new Okinawan HMSN-P-affected families (families 3 and 4 in Figure 1A) in our study. In total, 9 affected and 15 unaffected individuals from the Kansai area and four affected and four unaffected individuals from the Okinawa Islands were enrolled in the study. Written informed consent was obtained from

Table 1. Clinical Characteristics of Patients with HMSN-P from Families 1 and 2 from Kansai and Families 3 and 4 from Okinawa

		Family 3			Family 4
	Families 1 and 2	**III-12**	**III-14**	**III-15**	**III-4**
Age at examination (years)	40s–50s	54	52	50	54
Age at onset (years)	37.5 ± 8	44	40	early 20s	41
Initial symptoms	shoulder dislocation and difficulty walking	proximal leg weakness	painful cramps	painful cramps and fasciculation	painful cramps and calf atrophy
Motor					
Proximal muscle weakness and atrophy	+	+	mild	+	+
Painful cramps	+	+	+	+	+
Fasciculations	+	+	+	+	+
Motor ability	bedridden after 10–20 years from disease onset	unable to walk; wheelchair	only mild difficulty climbing stairs	walk with effort	unable to walk; wheelchair
Bulbar symptoms	− ~ +	−	−	−	−
Sensory					
Dysesthesia	+	+	mild	+	+
Decreased tactile sensation	+	+	−	mild	+
Decreased vibratory sensation	+	mild	mild	mild	+
Reflexes					
Tendon reflexes	diminished	diminished	diminished	diminished	diminished
Pathological reflexes	−	−	−	−	−
Laboratory Tests and Electrophysiological Findings					
Serum creatine kinase level	270 ± 101 IU/l	761 IU/l	not measured	625 IU/l	399 IU/l
Hyperglycemia	4/13 patients	−	−	−	+
Hyperlipidemia	3/13 patients	+	−	+	+
Nerve conduction study	motor and sensory axonal degeneration	motor and sensory axonal degeneration	not examined	not examined	motor and sensory axonal degeneration
Needle electromyography	neurogenic changes with fibrillation potentials and positive sharp waves	neurogenic changes with fibrillation potentials and positive sharp waves	not examined	not examined	not examined

The clinical characteristics of the patients from families 1 and 2 were summarized in accordance with the previous studies.[5,6]

all participants. This study was approved by the institutional review boards at the University of Tokyo and the Tokushima University Hospital. Genomic DNA was extracted from peripheral-blood leukocytes or an autopsied brain according to standard procedures.

The clinical presentations of the patients from the four families are summarized in Table 1 and Table S1, available online. Characteristic painful cramps and fasciculations were noted at the initial stage of the disease in all the patients from the four families. Whereas some of the patients showed painful cramps in their 20s, the ages of onset of motor weakness (41.6 ± 2.9 years old) were quite uniform. These patients presented slowly progressive, predominantly proximal weakness and atrophy with diminished tendon reflexes in the lower extremities. Sensory impairment was generally mild. Indeed, one patient (III-4 in family 4) has been diagnosed with very slowly progressive ALS. Although frontotemporal dementia (FTD) is an occasionally observed clinical presentation in patients with ALS, dementia was not observed in these patients. Laboratory tests showed mildly elevated serum creatine kinase levels. Electrophysiological studies showed similar results in all the patients investigated and revealed a decreased number of motor units with abundant positive sharp waves, fibrillation, and fasciculation potentials. Sensory-nerve action potentials of the sural nerve were lost in the later stage of the disease. All these clinical findings were similar to those described in previous reports.[1,3,4]

To further narrow the candidate region, we conducted detailed genotyping by employing the Genome-Wide Human SNP array 6.0 (Affymetrix). Multipoint parametric linkage analysis and haplotype reconstruction were performed with the pipeline software SNP-HiTLink[8] and Allegro v.2[9] (Figure 1A). In addition to the SNP genotyping, we also used newly discovered polymorphic dinucleotide repeats for haplotype comparison (microsatellite marker 1 [MS1], chr3: 101,901,207–101,901,249; and MS2, chr3: 102,157,749–102,157,795 in hg18) around *TFG* (see Table S2 for primer sequences). The genome-wide linkage study revealed only one chromosome 3 region showing a cumulative LOD score exceeding 3.0 (Figure 1B), confirming the result of our previous study.[7] An obligate recombination event was observed between rs4894942 and rs1104964, thus further refining the telomeric boundary of the candidate region in Kansai families (Figure 2A). The Okinawan families (families 3 and 4) shared an extended disease haplotype spanning 3.3 Mb, consistent with a founder effect reported in the Okinawan HMSN-P-affected families,[1] thus defining the 3.3 Mb region as the minimum candidate region.

We then performed exon capture (Sequence Capture Human Exome 2.1 M Array [NimbleGen]) of the index patient from family 3 and subsequent passively parallel sequencing by using two lanes of GAIIx (100 bp single end [Illumina]) and a one-fifth slide of SOLiD 4 (50 bp single end [Life Technologies]). GAIIx and SOLiD4 yielded 2.60 and 2.76 Gb of uniquely mapped reads,[10] respectively. The average coverages were 29.0× and 26.8× in GAIIx and SOLiD4, respectively (Table S3 and Figure S1). In summary, 175,236 single nucleotide variants (SNVs) and 25,987 small insertions/deletions were called.[11] The numbers of exonic and splice-site variants were 14,189 and 127, respectively. In the minimum candidate region of 3.3 Mb, only 11 exonic SNVs were found, and only one was novel (i.e., not found in dbSNP) and nonsynonymous. Direct nucleotide-sequence analysis confirmed the presence of heterozygous SNV c.854C>T (p.Pro285Leu) in TRK-fused gene (*TFG* [NM_006070.5]) in all the patients from families 3 and 4 (Figure 3A and Figure S2[12]). Intriguingly, direct nucleotide-sequence analysis of all *TFG* exons (see Table S4 for primer sequences) of one patient from each of families 1 and 2 from the Kansai area revealed an identical c.854C>T (p.Pro285Leu) *TFG* mutation cosegregating with the disease (Figure 1A and Figure 3A). The base substitution was not observed in 482 Japanese controls (964 chromosomes), dbSNP, the 1000 Genomes Project Database, or the Exome Sequencing Project Database. Pro285 is located in the P/Q-rich domain in the C-terminal region of TFG (Figure 3B) and is evolutionally conserved (Figure 3C). PolyPhen predicts it to be "probably damaging." Because some of the exonic sequences were not sufficiently covered by exome sequencing (i.e., their read depths were no more than 10×) (Figure S1), direct nucleotide-sequence analysis was further conducted for these exonic sequences (Table S5). However, it did not reveal any other novel nonsynonymous variants, confirming that c.854C>T (p.Pro285Leu) is the only mutation exclusively present in the candidate region of 3.3 Mb. All together, we concluded that it was the disease-causing mutation.

Because we found an identical mutation in both Kansai (families 1 and 2) and Okinawan (families 3 and 4) families, we then compared the haplotypes with the c.854C>T (p.Pro285Leu) mutation in the Kansai and Okinawan families in detail. To obtain high-resolution haplotypes, we included custom-made markers, including MS1 and MS2, and new SNVs identified by our exome analysis, in addition to the high-density SNPs used in the linkage analysis. The two Kansai families shared as long as 24.0 Mb of haplotype, and the two Okinawan families shared 3.3 Mb, strongly supporting a common ancestry in each region. When the haplotypes of the Kansai and Okinawan families were compared, it turned out that these families do not share the same haplotype because the markers nearest to *TFG* are discordant at markers 48.5 kb centromeric and 677 bp telomeric to the mutation within a haploblock (Figure 2B). Although the possibility of rare recombination events just distal to the mutation cannot be completely excluded, as suggested by the population-based recombination map (Figure 2B), these findings strongly support the interpretation that the mutations have independent origins and provide further evidence that *TFG* contains the causative mutation for this disease.

Mutational analyses of *TFG* were further conducted in patients with other diseases affecting lower motor neurons (including familial ALS [n = 18], axonal HMSN [n = 26], and hereditary motor neuropathy [n = 3]) and revealed no mutations in *TFG*, indicating that c.854C>T (p.Pro285-Leu) in *TFG* is highly specific to HMSN-P.

In this study, we identified in all four families a single variant that appears to have developed on two different haplotypes. The mutation disrupts the PXXP motif, also known as the Src homology 3 (SH3) domain, which might affect protein-protein interactions. In addition, substitution of leucine for proline is expected to markedly alter the protein's secondary structure, which might substantially compromise the physiological functions of TFG.

By employing the primers shown in Table S6, we obtained full-length cDNAs by PCR amplification of the cDNAs prepared from a cDNA library of the human fetal brain (Clontech). During this process, four species of cDNA were identified (Figure S3A). To determine the relative abundance of these cDNA species, we used the primers shown in Table S7 to conduct fragment analysis of the RT-PCR products obtained from RNAs extracted from various tissues; these primers were designed to discriminate four cDNA species on the basis of the size of the PCR products. The analysis revealed that TFG is ubiquitously expressed, including in the spinal cord and dorsal root ganglia, which are the affected sites of HMSN-P (Figure S3B).

Neuropathological studies were performed in a *TFG*-mutation-positive patient (IV-25 in family 1) who died of

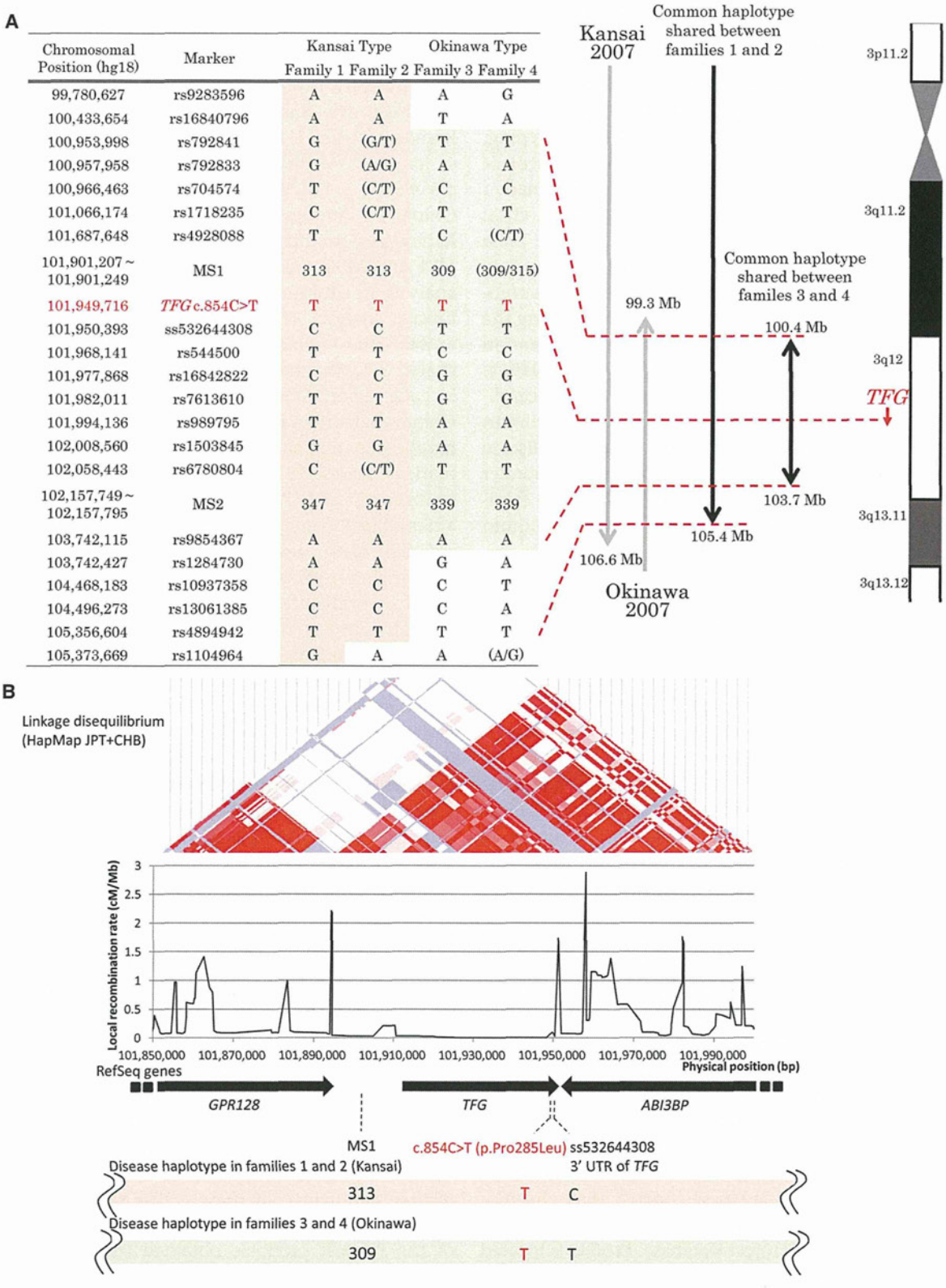

Figure 2. Haplotype Analysis and Minimum Candidate Region of HMSN-P
(A) Haplotypes were reconstructed for all the families with the use of SNP array data and microsatellite markers. Previously reported candidate regions are shown as "Kansai 2007" and "Okinawa 2007."[1,6] Because families 1 and 2 are distantly related, an extended shared common haplotype was observed on chromosome 3, as indicated by a previous study.[6] A reassessment of linkage analysis with high-density SNP markers revealed a recombination between rs4894942 and rs1104964 in family 2, thus refining the telomeric boundary of the candidate region in Kansai families (designated as "Common haplotype shared between families 1 and 2). Furthermore, a shared common haplotype (3.3 Mb with boundaries at rs16840796 and rs1284730) between families 3 and 4 was found, defining the minimum candidate region.

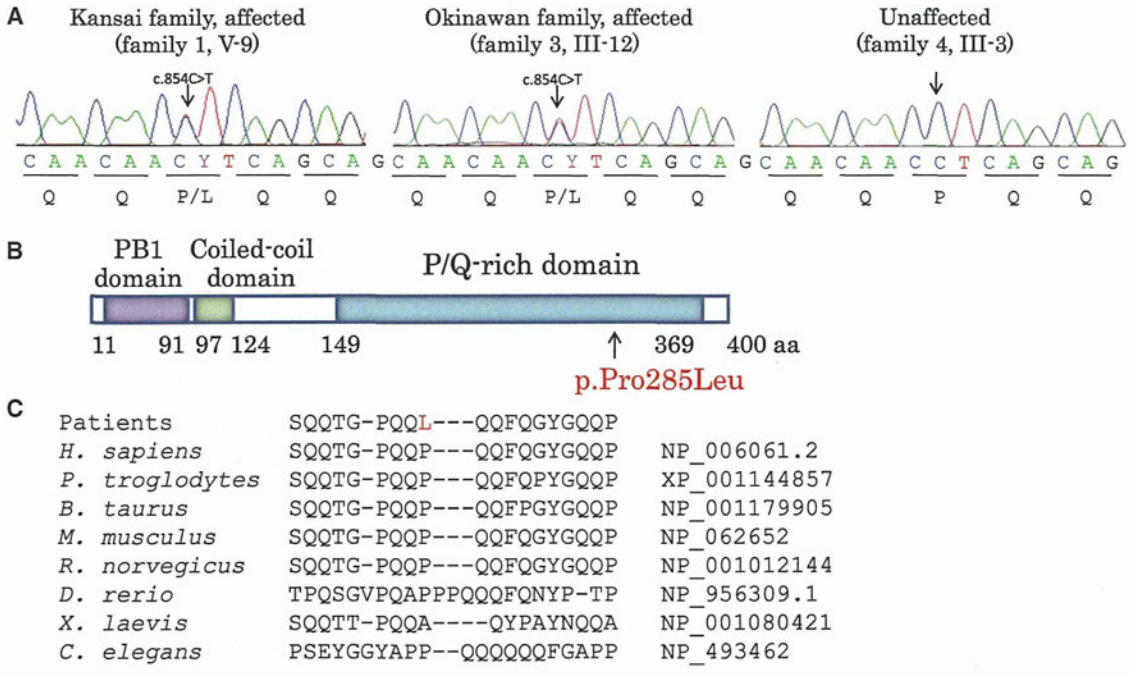

Figure 3. Identification of Causative Mutation

(A) Exome sequencing revealed that only one novel nonsynonymous variant is located within the minimum candidate region. Direct nucleotide-sequence analysis confirmed the mutation, c.854C>T (p.Pro285Leu), in *TFG* in both Kansai and Okinawan families. The mutation cosegregated with the disease (Figure 1A).

(B) Schematic representation of TFG isoform 1. The alteration (p.Pro285Leu) detected in this study is shown below.

(C) Cross-species homology search of the partial TFG amino acid sequence containing the p.Pro285Leu alteration revealed that Pro285 is evolutionally conserved among species.

pneumonia at 67 years of age.[5] Immunohistochemical observations employing a TFG antibody (Table S8) revealed fine granular immunostaining of TFG in the cytoplasm of motor neurons in the spinal cord of neurologically normal controls (n = 3; age at death = 58.7 ± 19.6 years old) (Figure 4A). In the HMSN-P patient, in contrast, TFG-immunopositive inclusion bodies were detected in the motor neurons of the facial, hypoglossal, and abducens nuclei and the spinal cord, as well as in the sensory neurons of the dorsal root ganglia, but were not detected in glial cells (Figures 4B–4D). A small number of cortical neurons in the precentral gyrus also showed TFG-immunopositive inclusion bodies (Figure 4E). Serial sections stained with antibodies against ubiquitin or TFG (Figure 4F) and double immunofluorescence staining (Figure 4G) demonstrated that TFG-immunopositive inclusions colocalized with ubiquitin deposition. Inclusion bodies were immunopositive for optineurin in motor neurons of the brainstem nuclei and the anterior horn of the spinal cord,[5] as well as in sensory neurons of the dorsal root ganglia (data not shown). These data strongly indicate that HMSN-P is a proteinopathy involving TFG.

Because HMSN-P and ALS share some clinical characteristics, we then examined whether neuropathological findings of HMSN-P shared cardinal features with those of sporadic ALS.[13–16] Immunohistochemistry with a TDP-43 antibody revealed skein-like inclusions in the remaining motor neurons of the abducens nucleus and the anterior horn of the lumbar cord (Figures 4H–4I). Phosphorylated TDP-43-positive inclusions were also identified in neurons of the anterior horn of the cervical cord and Clarke's nucleus (Figures 4J–4K). In contrast, TFG immunostaining of spinal-cord specimens from four patients with sporadic ALS (their age at death was 72.3 ± 7.4 years old) revealed no pathological staining in the motor neurons (data not shown). Double immunofluorescence staining revealed that many of the TFG-immunopositive round inclusions in the HSMN-P patient were negative for TDP-43 (Figure 4L), whereas a small number of inclusions were positive for both TFG and TDP-43 (Figure 4M). In addition, to investigate morphological Golgi-apparatus changes, which have recently been found in motor neurons of autopsied tissues of ALS patients,[17] we conducted immunohistochemical analysis by using

(B) Disease haplotypes in the Kansai and Okinawan kindreds are indicated below. Local recombination rates, RefSeq genes, and the linkage disequilibrium map from HapMap JPT (Japanese in Tokyo, Japan) and CHB (Han Chinese in Beijing, China) samples are shown above the disease haplotypes. When disease haplotypes of the Kansai and Okinawan kindreds are compared, the markers nearest to *TFG* are discordant at markers 48.5 kb centromeric and 677 bp telomeric to the mutation within a haploblock, strongly supporting the interpretation that the mutations have independent origins.

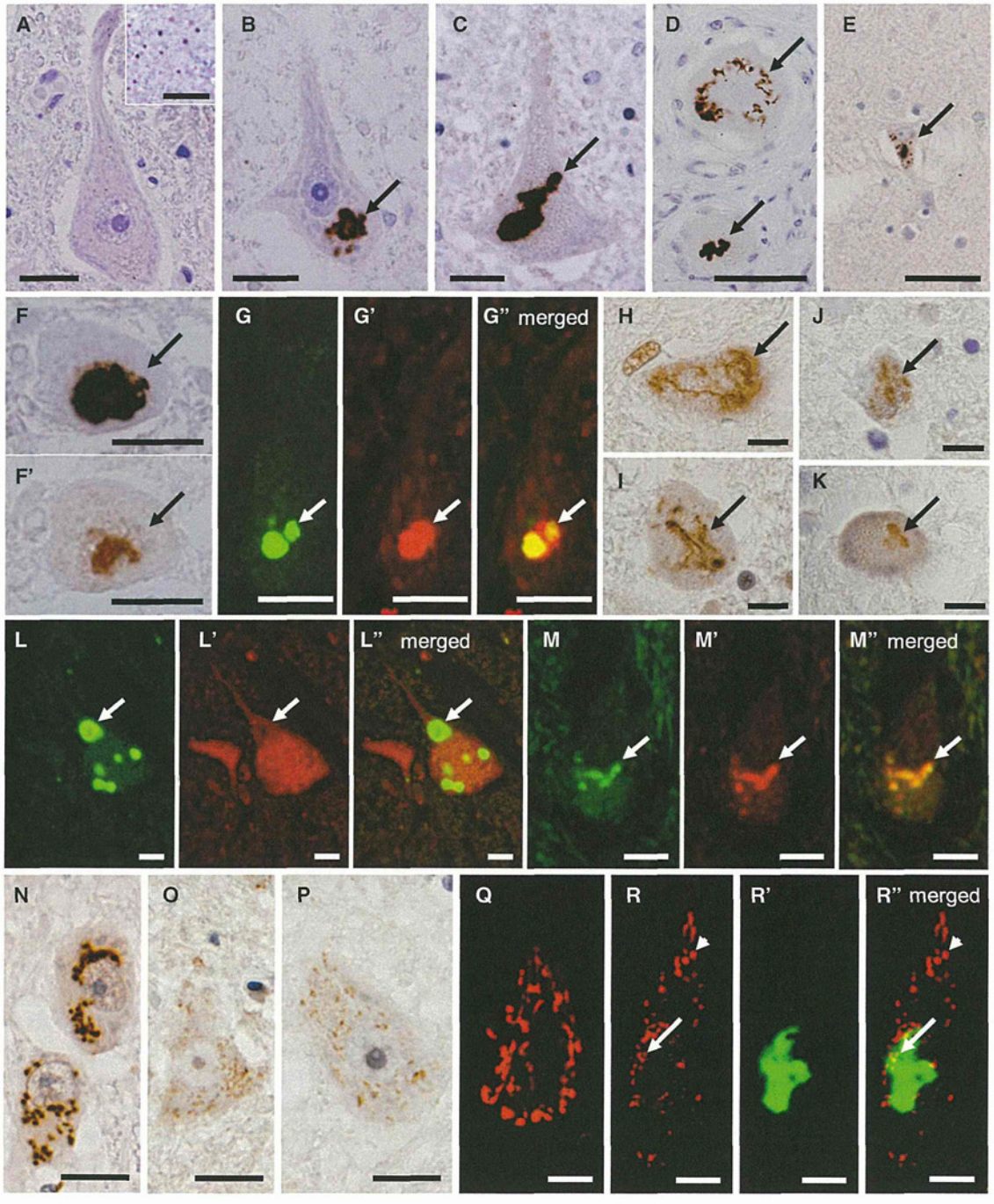

Figure 4. TFG-Related Neuropathological Findings

(A) TFG immunostaining (with hematoxylin counterstaining) of a motor neuron in the spinal cord of a neurologically normal control. A high-power magnified photomicrograph (inset) shows fine granular staining of TFG in the cytoplasm. The scale bars represent 20 μm (main panel) and 10 μm (inset).

(B–E) TFG-immunopositive inclusions of the neurons (with hematoxylin counterstaining) in the hypoglossal nucleus (B), anterior horn of the spinal cord (C), dorsal root ganglion (D, arrows), and motor cortex (E, arrow) of the patient with the *TFG* mutation. The scale bars represent 20 μm (B–D) and 50 μm (E).

(F and F′) Serial section analysis of the facial nucleus motor neuron showing an inclusion body colabeled for TFG (F) and ubiquitin (F′). The scale bars represent 20 μm.

(G–G″) Double immunofluorescence microscopy confirming colocalization of TFG (green) and ubiquitin (red) in an inclusion body of a motor neuron in the hypoglossal nucleus. The scale bars represent 20 μm.

(H and I) TDP-43-positive skein-like inclusions in the motor neurons of the abducens nucleus (H) and anterior horn of the lumbar cord (I). The scale bars represent 20 μm.

(J and K) Phosporylated TDP-43-positive inclusion bodies in the cervical anterior horn (J) and Clarke's nucleus (K). The scale bars represent 20 μm.

(L–L″) Round inclusions (arrows) positive for TFG (green) but negative for TDP-43 (red). The scale bars represent 20 μm.

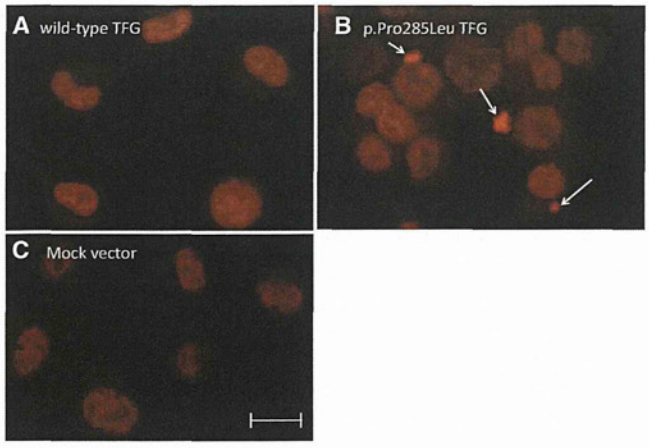

Figure 5. Formation of Cytoplasmic TDP-43 Aggregation Bodies in Cells Stably Expressing Mutant p.Pro285Leu TFG
The coding sequence of *TFG* cDNA was subcloned into pBluescript (Stratagene). After site-directed mutagenesis with a primer pair shown in Table S9, the mutant cDNAs were cloned into the BamHI and XhoI sites of pcDNA3 (Life Technologies). Stable cell lines were established by Lipofectamine (Life Technologies) transfection according to the manufacturer's instructions. Established cell lines were cultured under the ordinary cell-culture conditions (37°C and 5% CO_2) for 5–6 days and were subjected to immunocytochemical analyses. Neuro-2a cells stably expressing wild-type TFG (A), mutant TFG (p.Pro285Leu) (B), and a mock vector (C) are shown. TDP-43-immunopositive cytoplasmic inclusions are absent in the cells stably expressing wild-type TFG or the mock vector (A and C); however, TDP-43-immunopositive cytoplasmic inclusions were exclusively demonstrated in cells stably expressing mutant TFG (p.Pro285Leu), as indicated by arrows (B). Similar results were obtained with HEK 293 cells (not shown). Scale bars represent 10 μm.

a TGN46 antibody. It revealed that the Golgi apparatus was fragmented in approximately 70% of the remaining motor neurons in the lumbar anterior horn. The fragmentation of the Golgi apparatus was prominent near TFG-positive inclusion bodies (Figures 4N–4R). In summary, we found abnormal TDP-43-immunopositive inclusions in the cytoplasm of motor neurons, as well as fragmentation of the Golgi apparatus in HMSN-P, confirming the overlapping neuropathological features between HMSN-P and sporadic ALS.

To further investigate the effect of mutant TFG in cultured cells, stable cell lines expressing wild-type and mutant TFG (p.Pro285Leu) were established from neuro-2a and human embryonic kidney (HEK) 293 cells as previously described.[18] Established cell lines were cultured under the ordinary cell-culture conditions (37°C and 5% CO_2) for 5–6 days and were subjected to immunocytochemical analyses. The neuro-2a cells stably expressing wild-type or mutant TFG demonstrated no distinct difference in the distribution of endogenous TFG, FUS, or OPTN (data not shown). In contrast, cytoplasmic inclusions containing endogenous TDP-43 were exclusively observed in the neuro-2a cells stably expressing untagged mutant TFG, but not in those expressing wild-type TFG (Figure 5). Similar data were obtained from HEK 293 cells (data not shown). Thus, the expression of mutant TFG leads to mislocalization and inclusion-body formation of TDP-43 in cultured cells.

TFG was originally identified as a part of fusion oncoproteins (NTRK1-T3 in papillary thyroid carcinoma,[19] TFG-ALK in anaplastic large cell lymphoma,[20] and TFG/NOR1 in extraskeletal myxoid chondrosarcoma[21]), where the N-terminal portions of TFG are fused to the C terminus of tyrosine kinases or a superfamily of steroid-thyroid hormone-retinoid receptors acting as a transcriptional activator leading to the formation of oncogenic products. Very recently, TFG-1, a homolog of TFG in *Caenorhabditis elegans*, and TFG have been discovered to localize in endoplasmic-reticulum exit sites. TFG-1 acts in a hexameric form that binds the scaffolding protein Sec16 complex assembly and plays an important role in protein secretion with COPII-coated vesicles.[22] It is noteworthy that mutations in genes involved in vesicle trafficking[23,24] (such genes include *VAPB*, *CHMP2B*, *alsin*, *FIG4*, *VPS33B*, *PIP5K1C*, and *ERBB3*) cause motor neuron diseases, emphasizing the role of vesicle trafficking in motor neuron diseases. Thus, altered vesicle trafficking due to the *TFG* mutation might be involved in the motor neuron degeneration in HMSN-P. The presence of TFG-immunopositive inclusions in motor neurons raises the possibility that mutant TFG results in the misfolding and formation of cytoplasmic aggregate bodies, as well as altered vesicle trafficking.

An intriguing neuropathological finding is TDP-43-positive cytoplasmic inclusions in the motor neurons; these inclusions have recently been established as the fundamental neuropathological findings in ALS.[13,14] Of note, expression of mutant, but not wild-type, TFG in cultured cells led to the formation of TDP-43-containing cytoplasmic aggregation. These observations are similar

(M–M″) An inclusion immunopositive for both TFG (green) and TDP-43 (red) is observed in a small number of neurons. The scale bars represent 20 μm.
(N) Normal Golgi apparatus in the neurons of the intact thoracic intermediolateral nucleus. The scale bar represents 20 μm.
(O and P) Fragmentation of the Golgi apparatus with small, round, and disconnected profiles in the affected motor neurons of the lumbar anterior horn. The scale bars represent 20 μm.
(Q–R″) Immunohistochemical observations of the Golgi apparatus and TFG-immunopositive inclusions employing antibodies against TGN46 (red) and TFG (green), respectively. The scale bars represent 10 μm.
(Q) Normal size and distribution (red) in a motor neuron without inclusions.
(R–R″) The Golgi apparatus was fragmented into various sizes and reduced in number in the lumbar anterior horn motor neuron with TFG-positive inclusions (green). The fragmentation predominates near the inclusion (arrow), whereas the Golgi apparatuses distant from the inclusion showed nearly normal patterns (arrow head).

to what has been described for ALS, where TDP-43 is mislocalized from the normally localized nucleus to the cytoplasm with concomitant cytoplasmic inclusions. Cytoplasmic TDP-43 accumulation and inclusion formation have also been observed in motor neurons in familial ALS with mutations in *VAPB* (MIM 608627) or *CHMP2B* (MIM 600795).[25,26] Furthermore, TDP-43 pathology has been demonstrated in transgenic mice expressing mutant VAPB.[27] Although the mechanisms of mislocalization of TDP-43 remain to be elucidated, these observations suggest connections between alteration of vesicle trafficking and mislocalization of TDP-43. Thus, common pathophysiologic mechanisms might underlie motor neuron degenerations involving vesicle trafficking including TFG, as well as VAPB and CHMP2B. Because TDP-43 is an RNA-binding protein, RNA dysregulation has been suggested to play important roles in the TDP43-mediated neurodegeneration.[28] Furthermore, recent discovery of hexanucleotide repeat expansions in *C9ORF72* in familial and sporadic ALS/FTD (MIM 105550)[29,30] emphasizes the RNA-mediated toxicities as the causal mechanisms of neurodegeneration. Observations of TDP-43-positive cytoplasmic inclusions in the motor neurons of the patient with HMSN-P raise the possibility that RNA-mediated mechanisms might also be involved in motor neuron degeneration in HMSN-P.

In summary, we have found that *TFG* mutations cause HMSN-P. The presence of TFG/ubiquitin- and/or TDP-43-immunopositive cytoplasmic inclusions in motor neurons and cytosolic aggregation composed of TDP-43 in cultured cells expressing mutant TFG indicate a novel pathway of motor neuron death.

Supplemental Data

Supplemental Data include three figures and nine tables and can be found with this article online at http://www.cell.com/AJHG/.

Acknowledgments

The authors thank the families for participating in the study. We also thank the doctors who obtained clinical information of the patients. This work was supported in part by Grants-in-Aid for Scientific Research on Innovative Areas (22129002); the Global Centers of Excellence Program; the Integrated Database Project; Scientific Research (A) (B21406026) and Challenging Exploratory Research (23659458) from the Ministry of Education, Culture, Sports, Science, and Technology of Japan; a Grant-in-Aid for Research on Intractable Diseases and Comprehensive Research on Disability Health and Welfare from the Ministry of Health, Labour, and Welfare, Japan; Grants-in-Aid from the Research Committee of CNS Degenerative Diseases; the Ministry of Health, Labour, and Welfare of Japan; the Charcot-Marie-Tooth Association; and the National Medical Research Council of Australia. H.I. was supported by a Research Fellowship from the Japan Society for the Promotion of Science for Young Scientists. We also thank S. Ogawa (Cancer Genomics Project, The University of Tokyo) for his kind help in the analyses employing GAIIx and SOLiD4.

Received: April 16, 2012
Revised: May 27, 2012
Accepted: July 2, 2012
Published online: August 9, 2012

Web Resources

The URLs for data presented herein are as follows.

1000 Genomes Project Database, http://www.1000genomes.org/
dbSNP, http://www.ncbi.nlm.nih.gov/projects/SNP/
HapMap, http://hapmap.ncbi.nlm.nih.gov/
NHLBI GO Exome Sequencing Project, https://esp.gs.washington.edu/drupal/
Online Mendelian Inheritance in Man (OMIM), http://www.omim.org
PolyPhen, http://genetics.bwh.harvard.edu/pph/
RefSeq, http://www.ncbi.nlm.nih.gov/projects/RefSeq/
UCSC Human Genome Browser, http://genome.ucsc.edu/

References

1. Takashima, H., Nakagawa, M., Nakahara, K., Suehara, M., Matsuzaki, T., Higuchi, I., Higa, H., Arimura, K., Iwamasa, T., Izumo, S., and Osame, M. (1997). A new type of hereditary motor and sensory neuropathy linked to chromosome 3. Ann. Neurol. *41*, 771–780.
2. Nakagawa, M. (2009). [Wide spectrum of hereditary motor sensory neuropathy (HMSN)]. Rinsho Shinkeigaku *49*, 950–952.
3. Maeda, K., Sugiura, M., Kato, H., Sanada, M., Kawai, H., and Yasuda, H. (2007). Hereditary motor and sensory neuropathy (proximal dominant form, HMSN-P) among Brazilians of Japanese ancestry. Clin. Neurol. Neurosurg. *109*, 830–832.
4. Patroclo, C.B., Lino, A.M., Marchiori, P.E., Brotto, M.W., and Hirata, M.T. (2009). Autosomal dominant HMSN with proximal involvement: new Brazilian cases. Arq. Neuropsiquiatr. *67* (3B), 892–896.
5. Fujita, K., Yoshida, M., Sako, W., Maeda, K., Hashizume, Y., Goto, S., Sobue, G., Izumi, Y., and Kaji, R. (2011). Brainstem and spinal cord motor neuron involvement with optineurin inclusions in proximal-dominant hereditary motor and sensory neuropathy. J. Neurol. Neurosurg. Psychiatry *82*, 1402–1403.
6. Takahashi, H., Makifuchi, T., Nakano, R., Sato, S., Inuzuka, T., Sakimura, K., Mishina, M., Honma, Y., Tsuji, S., and Ikuta, F. (1994). Familial amyotrophic lateral sclerosis with a mutation in the Cu/Zn superoxide dismutase gene. Acta Neuropathol. *88*, 185–188.
7. Maeda, K., Kaji, R., Yasuno, K., Jambaldorj, J., Nodera, H., Takashima, H., Nakagawa, M., Makino, S., and Tamiya, G. (2007). Refinement of a locus for autosomal dominant hereditary motor and sensory neuropathy with proximal dominancy (HMSN-P) and genetic heterogeneity. J. Hum. Genet. *52*, 907–914.
8. Fukuda, Y., Nakahara, Y., Date, H., Takahashi, Y., Goto, J., Miyashita, A., Kuwano, R., Adachi, H., Nakamura, E., and Tsuji, S. (2009). SNP HiTLink: A high-throughput linkage analysis system employing dense SNP data. BMC Bioinformatics *10*, 121.
9. Gudbjartsson, D.F., Thorvaldsson, T., Kong, A., Gunnarsson, G., and Ingolfsdottir, A. (2005). Allegro version 2. Nat. Genet. *37*, 1015–1016.